Gait & Posture 29 (2009) 658–660

Contents lists available at ScienceDirect

Gait & Posture

journal homepage: www.elsevier.com/locate/gaitpost

Short communication

Olfactory stimuli and enhanced postural stability in older adults

Shannon Freeman [a,b], Satoru Ebihara [a,*], Takae Ebihara [a], Kaijun Niu [a], Masahiro Kohzuki [b], Hiroyuki Arai [a], James P. Butler [a,c]

[a] Department of Geriatrics and Gerontology, Institute of Development, Aging and Cancer, Tohoku University, Seiryo-machi 4-1, Aoba-ku, Sendai 980-8575, Japan
[b] Department of Internal Medicine and Rehabilitation Science, Tohoku University Graduate School of Medicine, Seiryo-machi 1-1, Aoba-ku, Sendai 980-8574, Japan
[c] Program in Molecular and Integrative Physiological Sciences, Harvard School of Public Health, Boston, MA 02115, USA

ARTICLE INFO

Article history:
Received 15 October 2008
Received in revised form 10 February 2009
Accepted 11 February 2009

Keywords:
Black pepper
Lavender
Balance
Force plate
Trajectory length

ABSTRACT

Ameliorating postural instability is an important component of geriatric health care. The effect of olfactory stimuli (lavender and black pepper oils) on postural control in 17 older adults (78 ± 6 years old) who had no apparent neurological deficits was studied. Measurements of center of pressure (CoP) trajectories were done with subjects standing quietly on a force plate. Control measurements were compared with olfactory interventions: brief exposure to sham (distilled water), lavender oil, and black pepper oil; experiments were repeated with eyes open and eyes closed. From the CoP data, the root mean square (RMS) displacement and velocity in mediolateral (ML) and antero-posterior (AP) directions, and the total trajectory length were computed. This study found that with eyes closed, olfactory stimulation with either lavender or black pepper oil significantly decreased both ML and AP RMS velocities and trajectory lengths compared with baseline. In contrast, little effect was observed under the eyes-open condition. Decreases in RMS displacements were small and mostly insignificant. The study suggests that olfactory stimulation may improve posture stability in older adults through decreasing the velocities of postural adjustments during normal sway.

1. Introduction

Increased postural instability in older adults is well established [1,2], and increased postural sway has been associated with the incidence of falls in older adults [3,4]. Many factors contribute to loss in balance control, including diminished vision, muscle weakness, vestibular disorders, bone integrity, spinal injury, and somatosensory deficit [5].

It has traditionally been thought that balance control occurs at an autonomic level, involving a complex interplay between vision and noncortical polysynaptic brainstem pathways associated with the vestibular apparatus and proprioception [6,7]. However, recent research has suggested that the cerebral cortex may be involved in controlling specific aspects of balance [8]. Odor is one of the strongest stimuli over a wide range of the cerebral cortex [9]. Moreover, there are brain diseases, such as Alzheimer's, schizophrenia, and certain types of stroke, which manifest both olfactory dysfunction and balance instability [10–12], suggesting that both neuronal deficits may linked. However, data are lacking regarding the relationship between olfactory stimulation and postural stability. In order to investigate this, we gave odor stimuli using black pepper and lavender oils to subjects, and measured several indices of postural stability.

2. Methods

2.1. Subjects

We used posters to recruit community-dwelling older adult participants from communities surrounding Sendai, Japan. Seventeen subjects, age 78 ± 6 years, male/female ratio of 13/4, completed the study. The experimental protocol (2007-192) was approved by the institutional ethics committee, and verbal informed consent was obtained from each subject. Criteria for participation included being medically stable, adequately comprehending instructions and the nature of the study, and being able to stand up and walk independently without a cane or assistance device. Functional independence was assessed with the Barthel Index (subject range 80–95). Exclusion criteria included evidence of arthritis in the lower limbs, chronic back, knee or hip joint pain, evidence of Parkinson's disease, Meniere syndrome, cerebellar signs, cognitive deficits (Mini-Mental State Examination: MMSE < 24), or peripheral neuropathy under standard neuropsychological assessment.

2.2. Protocol

Black pepper and lavender oils (#T03218 and #060706) were purchased from Yamamoto Perfumery Co., Osaka, Japan. Trials were conducted between 10:00 a.m. and 11:00 a.m. on separate days (minimum 2-day separation) to minimize a placebo or learning effect, as well as to insure stimulus clearance and a return to olfactory baseline. The order of the two oil and one sham trial exposures were randomly selected for each subject.

Subjects were instructed to stand with their feet slightly apart on a force plate. For each stimulus, the protocol was: 1 min eyes-open control trial, 2 min break,

* Corresponding author. Tel.: +81 22 717 7182; fax: +81 22 717 8498.
E-mail address: sebihara@idac.tohoku.ac.jp (S. Ebihara).

0966-6362/$ – see front matter © 2009 Elsevier B.V. All rights reserved.
doi:10.1016/j.gaitpost.2009.02.005

1 min eyes-closed control trial, 4 min break, 1 min eyes-open stimulus trial, 2 min break, 1 min eyes-closed stimulus trial. For the stimuli, an investigator held a paper stick, previously dipped in one of the oils or in distilled water, within a few centimeters of, but not touching, the right side of the subject's nose. The stick was re-dipped prior to each trial or corresponding break and held continuously from the time of exposure to the end of the eyes-closed stimulus trial. During eyes-open trials, subjects were instructed to look straight ahead. During the breaks, which were given to avoid fatigue, subjects were instructed to sit and relax. These were not blind studies, as the odor of the oils (and its absence in the shams) was more than sufficient for detection by all subjects.

2.3. Measurements

Movement of the body center of pressure (CoP) was measured with a force plate (Gravicoda GS-2000, Anima, Tokyo). Signals from its three force transducers were sampled at 100 Hz, obtaining individual 4096 long data strings, over 41 s periods during each trial. The data were filtered and compressed with a 9-point Gaussian filter using central binomial coefficient weighting. For each set of data, comprising six combinations of independent variables (three interventions and two visual conditions), the mediolateral (ML) and antero-posterior (AP) components of the CoP were computed. We derived five indices from these data: the total trajectory length; the root mean square displacements (RMSdisp) of the CoP (ML and AP), and the RMS velocities (RMSvel) of the CoP (ML and AP).

Variations among the control measurements by interventions were assessed by ANOVA with the Tukey post hoc test. Tests of the null hypothesis of no change relative to baseline were assessed with a paired two-tailed Student's *t*-test. Significance was taken at $p = 0.05$.

3. Results

Table 1 shows the population means ± S.D. of the raw dimensional quantities measured. ANOVA revealed no significant differences in the control measurements with the different interventions, so these data were pooled.

Among the 30 combinations of measurements, the most consistent results were in the eyes-closed group, where we found, for both lavender and the black pepper stimuli, significant fractional decreases in RMSvel (ML and AP), and in total trajectory length. Fig. 1 shows these results. With three exceptions, no other condition rose to statistical significance. These were: %change in RMSdisp (eyes-closed, AP, lavender); RMSdisp (eyes-open, AP, lavender); and RMSvel (eyes-open, AP, sham). However, as these follow no consistent pattern, we speculate that they may be secondary to the small sample size in this study, and are of little physiological significance. Surprisingly, and contrary to our initial expectations, we found no consistent pattern of significant decrease in the RMS displacement of the CoP.

4. Discussion

This is the first study to investigate the relationship between olfactory stimulation and postural stability in older adults. In the current study, both black pepper and lavender improved the balance parameters such as RMSvel and trajectory length, suggesting that the posture stabilizing effect of olfactory stimulation is not odor specific. This is in contrast to the observation that

Table 1
Pooled control values for postural stability indices based on center of pressure (CoP) measurements. RMSdisp and RMSvel: respectively root mean square displacement and velocity of CoP along the indicated axis. Traj length: total trajectory length of the CoP over the trial. ML: mediolateral, AP: antero-posterior. Data shown as means ± S.D., $N = 17$.

Postural stability index	Directional axis	Visual condition: eyes-open	Visual condition: eyes-closed
RMSdisp (cm)	ML	0.51 ± 0.17	0.73 ± 0.25
	AP	0.53 ± 0.19	0.71 ± 0.21
RMSvel (cm/s)	ML	1.54 ± 0.62	3.02 ± 1.40
	AP	1.40 ± 0.61	2.56 ± 1.13
Traj length (cm)	N/A	85 ± 38	156 ± 69

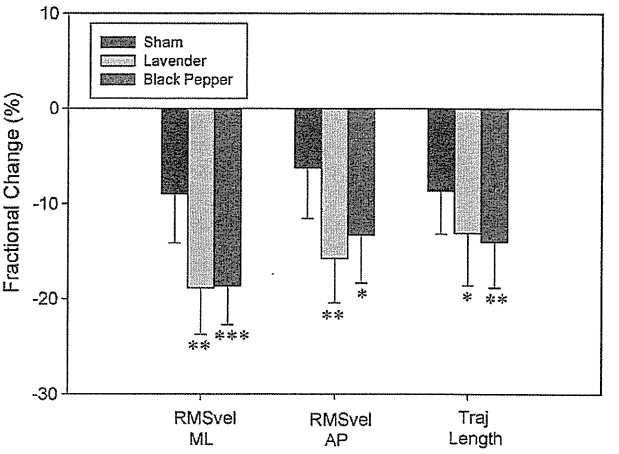

Fig. 1. Effects of odor stimulation on three posture stability indices under eyes-closed conditions. (With eyes open, neither olfactory stimulus showed any significant changes; data not shown.) Fractional changes are shown for RMS velocity in the mediolateral (ML) and antero-posterior (AP) directions, and for total trajectory length over the trial (Traj length). Data shown as means ± S.E. Significance levels: $^{*}p < 0.05$; $^{**}p < 0.01$; $^{***}p < 0.001$. The sham exposures did not reach statistical significance.

black pepper odor improved the swallowing reflex in dysphagic older adults whereas lavender oil did not [13].

It has previously been reported that poor balance with eyes closed is associated with an increased risk of falls [1,14], suggesting that the improvement of the balance with olfactory stimulation that we observed in similar conditions may be extrapolated to improving risk of falling in older people. This is in addition to the observation that aromatherapy with lavender has successful application in the treatment of behavioural and psychological symptoms of dementia [15].

The olfactory pathways project from the olfactory bulb widely throughout the cerebral cortex [16,17], although these studies were done in macaque monkeys. While there are important species differences, the fact that these are primates suggests an analogous projection may exist in humans. Moreover, it has recently been noted that the cerebral cortex is involved in upright posture maintenance in humans, especially in balance compensation mechanisms [5]. For instance, the insular cortex is importantly involved in the processing and integration of sensory information for balance [5], and is also activated by olfactory stimuli [13]. This suggests a mechanism by which odor stimulation may enhance cortical control of balance in older adults. This preliminary work thus suggests that odor stimulation may help ameliorate impairment of balance control in older adults, but further studies are necessary to apply these findings in practice.

Acknowledgments

This study was supported by grants 18-006 and 18-031 from the Japanese Ministry of Health, Labor, and Welfare, and by the Mitsui Sumitomo Insurance Welfare Foundation.

Conflict of interest statement

We declare that there are no financial or other conflicts of interest in relation to this work.

References

[1] Laughton CA, Slavin M, Katdare K, Nolan L, Bean JF, Kerrigan DC, et al. Aging, muscle activity, and balance control: physiologic changes associated with balance impairment. Gait Posture 2003;18:101–8.

[2] Baloh RW, Fife TD, Zwerling L, Socotch T, Jacobson K, Bell T, et al. Comparison of static and dynamic posturography in young and older normal people. J Am Geriatr Soc 1994;42:405–12.
[3] Fernie GR, Gryfe CI, Holliday PI, Llewellyn A. The relationship of postural sway in standing to the incidence of falls in geriatric subjects. Age Ageing 1982;11: 11–6.
[4] Maki BE, Holliday PJ, Topper AK. A prospective study of postural balance and risk of falling in an ambulatory and independent elderly population. J Gerontol 1994;49:M72–84.
[5] Jacob JV, Horak FB. Cortical control of postural responses. J Neural Transm 2007;114:1339–48.
[6] Dietz V. Human neuronal control of automatic functional movements: interaction. Physiol Rev 1992;72:33–69.
[7] Horak FB, MacPherson JM. Postural orientation and equilibrium. In: Handbook of Physiology. Exercise: regulation and integration of multiple systems. New York: Oxford University Press; 1996.
[8] Maki RE, McIlroy WE. Cognitive demands and cortical control of human balance-recovery reactions. J Neural Transm 2007;114:1274–96.
[9] De Araujo IE, Rolls ET, Velazco MI, Margot C, Cayeux I. Cognitive modulation of olfactory processing. Neuron 2005;46:671–9.
[10] Nakamura T, Meguro K, Yamazaki H, Okuzumi H, Tanaka A, Horikawa A, et al. Postural and gait disturbance correlated with decrease frontal cerebral blood flow in Alzheimer Disease. Alzheimer Dis Assoc Disord 1997;11:132–9.
[11] Marvel CL, Schwartz BL, Rosse RB. A quantitative measure of postural sway deficits in schizophrenia. Schizophrenia Res 2004;68:363–72.
[12] Di Fabio RP, Badke MB. Stance duration under sensory conflict conditions in patients with hemiplegia. Arch Phys Med Rehabil 1991;72:292–5.
[13] Ebihara T, Ebihara S, Maruyama M, Kobayashi M, Itou A, Arai H, et al. A randomized trial of olfactory stimulation using black pepper oil in older people with swallowing dysfunction. J Am Geriatr Soc 2006;54:1401–6.
[14] Sohng KY, Moon JS, Song HH, Lee KS, Kim YS. Risk factors for falls among the community-dwelling elderly in Korea. Taehan Kanho Hakhoe Chi (J Korean Acad Nurs) 2004;34(8):1483–90.
[15] Lin PW, Chan W, Ng BF, Lam LC. Efficacy of aromatherapy (*Lavandula angustifolia*) as an intervention for agitated behaviours in Chinese older persons with dementia: a cross-over randomized trial. Int J Geriatr Psychiatry 2007;22:405–10.
[16] Carmichael ST, Price JL. Architectonic subdivision of the orbital and medial prefrontal cortex in the macaque monkey. J Comp Neurol 1994;346:366–402.
[17] Ongur D, Price JL. Prefrontal cortical projections to the hypothalamus in macaque monkeys. J Comp Neurol 1998;401:480–505.

blood

2009 113: 3631-3639
Prepublished online Feb 13, 2009;
doi:10.1182/blood-2008-07-170381

Role of ephrinB2 in nonproductive angiogenesis induced by Delta-like 4 blockade

Shinsuke Yamanda, Satoru Ebihara, Masanori Asada, Tatsuma Okazaki, Kaijun Niu, Takae Ebihara, Akemi Koyanagi, Noriko Yamaguchi, Hideo Yagita and Hiroyuki Arai

Blood (print ISSN 0006-4971, online ISSN 1528-0020), is published semimonthly by the American Society of Hematology, 1900 M St, NW, Suite 200, Washington DC 20036.

Role of ephrinB2 in nonproductive angiogenesis induced by Delta-like 4 blockade

Shinsuke Yamanda,[1] Satoru Ebihara,[1] Masanori Asada,[1] Tatsuma Okazaki,[1] Kaijun Niu,[1] Takae Ebihara,[1] Akemi Koyanagi,[2] Noriko Yamaguchi,[3] Hideo Yagita,[3] and Hiroyuki Arai[1]

[1]Department of Geriatrics and Gerontology, Institute of Development, Aging and Cancer, Tohoku University, Sendai, Japan; [2]Division of Cell Biology and [3]Department of Immunology, Juntendo University School of Medicine, Tokyo, Japan

Delta-like 4 (DLL4) is one of the Notch ligands and plays an important role in vascular development. DLL4 blockade inhibits tumor growth by promoting nonproductive angiogenesis, which is characterized by an increase in vascular density and decrease in tissue perfusion. However, a detailed mechanism remains unclear. In this study, newly developed neutralizing antibodies against mouse and human DLL4 were used to investigate the possible involvement of VEGF-DLL4-ephrinB2 cascade in nonproductive angiogenesis caused by DLL4 blockade. DLL4 blockade and soluble ephrinB2 treatment suppressed tumor growth and induced nonproductive angiogenesis. DLL4 was expressed in subcutaneous tumors, and DLL4 blockade suppressed ephrinB2 expression in the tumors. DLL4 blockade significantly promoted human umbilical vein endothelial cell (HUVEC) proliferation in vitro, and the effect was additive to that of VEGF. Both DLL4 blockade and VEGF significantly increased cord length and branch points in a tubular formation assay. Expression of ephrinB2 in HUVECs was enhanced by VEGF alone, and the enhancement was inhibited by DLL4 blockade. Moreover, when we studied the effect of ephrinB2 RNA interference on HUVEC tubular formation, knockdown of ephrinB2 mimicked the effect of DLL4. These results suggest that ephrinB2 plays a crucial role in nonproductive angiogenesis caused by DLL4 blockade. (Blood. 2009;113:3631-3639)

Introduction

Tumor angiogenesis is an important process in solid tumor growth.[1] Growing tumors stimulate neovascularization through the secretion of proangiogenic growth factors, in particular, basic fibroblast growth factor and vascular endothelial growth factor (VEGF).[2] Based on accumulated studies concerning VEGF in tumor angiogenesis, anti-VEGF inhibitors such as bevacizumab, sunitinib, and sorafenib have been approved for clinical treatment of solid tumors in humans.[3]

Notch signals are evolutionarily conserved signaling mechanisms for intercellular communication and cell fate decision.[4] Four Notch receptors (Notch1, 2, 3, 4) and 5 ligands (Jagged 1 and 2, and Delta-like 1, 3, and 4) have been identified in mammals.[5,6] Once the ligand binds to the Notch receptor, it triggers the proteolytic release of the Notch intracellular domain, which translocates into the nucleus to form a nuclear complex with the transcription factor CSL (CBF1/RBP-j/Su(H)/Lag-1) and activates transcription of the downstream target gene. The hairy/enhancer of Split (HES1, 5, and 7) and the HES-related proteins (HEY1 and 2 and HEYL) are the main target genes of the Notch signaling in mammals.[7-9]

Several observations indicate that Notch signaling plays a critical role in vascular development.[10-12] Notch1 and Notch4 genes are expressed in endothelial cells within the embryonic vasculature, and Notch1 alone– or Notch1 plus Notch4–deficient mice display a severe defect in angiogenic vascular remodeling.[13-15] Overexpression of Notch4 also causes vascular abnormalities.[16] These observations suggest that an optimal range of Notch signaling is required for vascular development.

Delta-like 4 (DLL4) is the most recently identified Notch ligand and was found to interact with Notch1 and Notch4.[17,18] Haploinsufficiency of DLL4 produces severe vascular abnormalities that result in embryonic lethality.[19,20] Although many genes are involved in the developing vasculature, except for the VEGF gene, DLL4 is the only gene whose haploinsufficiency leads to major vascular defects and embryonic lethality.[21]

Notch signaling regulates not only embryonic vasculature but also tumor angiogenesis. Notch1, Notch4, Jagged1, and DLL4 are reported to participate in tumor angiogenesis.[22] Especially, DLL4 is highly expressed in human clear-cell renal cell carcinomas, bladder cancers, and breast cancers, and its interaction with VEGF is reported.[22-26] Therefore, DLL4 is expected to be a potentially important target of antiangiogenic therapy.

Eph receptor tyrosine kinases and their membrane-bound ephrin ligands mediate various cell-to-cell communications by bidirectional signaling and are involved in numerous developmental processes.[27] Eph receptors have been divided in 2 subclasses, classes A and B, depending on the type of interaction with the ephrin ligands.[28,29] In general, Eph class A receptors (EphA) bind to GPI-anchored ephrin ligands (ephrinA), whereas Eph class B receptors (EphB) bind to ephrin ligands containing transmembrane domain (ephrinB).[28,29] In vascular development, ephrinB2 and its cognate receptor EphB have attracted the most interest, because their homozygous mutation results in embryonic lethality.[30,31] EphrinB2 is expressed mainly on arterial endothelial cells, whereas venous endothelial cells express EphB4 as its main receptor.[32] Recently, ephrinB2 was reported to be involved in the maturation of tumor blood vessels.[26,33-35]

It has been described that VEGF induces the expression of DLL4 in endothelial cells and DLL4 up-regulates ephrinB2

Submitted July 23, 2008; accepted February 4, 2009. Prepublished online as *Blood* First Edition paper, February 13, 2009; DOI 10.1182/blood-2008-07-170381.

The publication costs of this article were defrayed in part by page charge payment. Therefore, and solely to indicate this fact, this article is hereby marked "advertisement" in accordance with 18 USC section 1734.

expression in both physiological and pathological conditions.[26,36-40] This VEGF-DLL4-ephrinB2 cascade is reported in transgenic mice developing hepatocarcinoma.[26] Recently, several groups have reported that the DLL4 blockade inhibits tumor growth by inducing nonproductive angiogenesis manifested by an increased tumor vascular density but a decreased tissue perfusion. However, the precise mechanism has not been elucidated.[41-44]

In this study, whether the VEGF-DLL4-ephrinB2 cascade plays an important role in the antitumor effect of DLL4 blockade and the nonproductive angiogenesis in vivo and in vitro was investigated.

Methods

Reagents

An anti–mouse DLL4 mAb (HMD4-2, hamster IgG) was generated by immunizing an Armenian hamster with recombinant mouse DLL4 (R&D Systems, Minneapolis, MN) and screening mAbs that blocked rat Notch1-Fc (R&D Systems) binding to mouse DLL4-expressing CHO cells (provided by Dr S. Chiba at Tokyo University, Tokyo, Japan). The anti–human DLL4 mAb (MHD4-46, mouse IgG1) was generated by immunizing a BALB/c mouse with recombinant human DLL4 (R&D Systems) and screening mAbs that blocked human Notch1-Fc (R&D Systems) binding to human DLL4-expressing CHO cells (provided by Dr S. Chiba). The anti–human Notch1 mAb (MHN1-519, mouse IgG1) was generated by immunizing a BALB/c mouse with recombinant human Notch1-Fc (R&D Systems). The following antibodies were used for Western blotting or immunohistochemistry: anti-factor VIII–related antigen antibody (DAKO, Carpinteria, CA), rabbit antiephrinB2 antibody (Santa Cruz Biotechnology, Santa Cruz, CA) for Western blotting, goat antiephrinB2 antibody (R&D Systems) for immunohistochemistry, rabbit anti-EphB4 antibody (Santa Cruz Biotechnology), anti–β-actin antibody (R&D Systems), and hypoxyprobe-1 (Chemicon, Temecula, CA). Recombinant human VEGF and recombinant mouse ephrinB2-Fc were purchased from R&D Systems.

Cell cultures

A lung squamous cell carcinoma cell line KLN205 was obtained from Cell Resource Center for Biomedical Research, Institute of Development, Aging and Cancer, Tohoku University, and a Lewis lung carcinoma cell line (LLC) was purchased from ATCC (Rockville, MD). KLN205 cells were cultured in MEM (Life Technologies, Gaithersburg, MD) supplemented with 10% FBS, 1% NEAA, and antibiotics. LLC cells were cultured in DMEM (Life Technologies) supplemented with 10% FBS and antibiotics. Human umbilical vein endothelial cells (HUVECs) and human microvascular endothelial cells (HMVECs) were purchased from Kurabo (Osaka, Japan). HUVECs were cultured in HuMedia-EG2 (Kurabo) containing 2% FCS. HMVECs were cultured in HuMedia-MvG (Kurabo) containing 5% FCS. Both HUVECs and HMVECs were used at passage 4 or below.

Mouse tumor models

KLN205 cells (5×10^5/animal) were implanted subcutaneously into the flank of male 6-week-old BDF1 mice on day 0. LLC cells (3×10^5 cells/animal) were implanted into the male 6-week-old C57BL/6 mice in the same way. Mice that received an implant of KLN205 cells were randomly allocated into 4 groups. Two groups received an intraperitoneal injection of HMD4-2 (0.25 mg/day per animal) or control hamster IgG (0.25 mg/day per animal) every 3 days from day 6, another 2 groups received intratumoral injection of recombinant mouse ephrinB2-Fc (0.1 mg/day per animal) or control human IgG (0.1 mg/day per animal) every other day from day 20. Mice that received an implant of LLC cells were randomly allocated into 3 groups. Each group received an intraperitoneal injection of high-dose HMD4-2 (1.0 mg/day per animal), low-dose HMD4-2 (0.25 mg/day per animal), or control hamster IgG (0.25 mg/day per animal) every 3 days from day 6. Half of the mice in each group were killed at the intended day, that is, when the diameter of the tumor became approximately 1 cm for HMD4-2 experiments and approximately 1.5 cm for soluble epheinB2 experiments, and then the tumors were removed and immediately frozen with liquid nitrogen or fixed in 10% neutral buffered formalin. The rest of mice were killed at day 36 in mice that received an implant of KLN205 cells, and at day 25 in mice that received an implant of LLC cells. All animal studies were performed with the permission of the Regional Council of Tohoku University and conformed to the Guide for the Care and Use of Laboratory Animals.[45]

RNA isolation and reverse-transcription–PCR

Total RNA was extracted from the subcutaneous tumors, and from cultured HUVECs stimulated with or without VEGF, KLN205 cells, and LLC cells using Iso-gene (Nippongene, Osaka, Japan) according to the manufacturer's instructions. First-strand cDNA was synthesized from RNA (1 μg) using a One-Step RNA PCR Kit (Takara, Shiga, Japan). The following primers were used for polymerase chain reaction (PCR): human DLL4 forward (5′-GACCACTTCGGCCACTATGT-3′), reverse (5′-CCTGTCCACTTTCTTCTCG-3′); murine DLL4 forward (5′-AGCTGGAAGTGGACTGTGGT-3′), reverse (5-TAGAGTCCCTGGGAGAGCAA-3′); human Notch1 forward (5′-CAGGCAATCCGAGGACTATG-3′), reverse (5′-CAGGCGTGTTGTTCTCACAG-3′); human Notch4 forward (5′-CACTGAGCCAAGGCATAGAC-3′), reverse (5′-ATCTCCACCTCACACCACTG-3′); human β-actin forward (5′-CATCACCATTGGCAATGAGC-3′), reverse (5′-CGATCCACACGGAGTACTTG-3′); and murine GAPDH forward (5′-CACCACCATGGAGAAGGCCGGG-3′), reverse (5′-GTGTAGCCCAAGATGCCCTTCA-3′).

Western blot analysis

HUVECs (5×10^5) and HMVECs (8×10^5) were plated onto 10-mm collagen-coated culture dishes in HuMedia-EBM (Kurabo) containing 0.1% FCS for 16 hours, and stimulated with 100 ng/mL VEGF for 6 hours. Then the medium was exchanged, and the HUVECs and HMVECs were treated with MHD4-46 or control mouse IgG (50 μg/mL) for 12 hours. The cells were lysed in ice-cold radioimmunoprecipitation assay (RIPA) buffer (0.5 mL). Minced tumors (0.2 mg) were lysed in ice-cold RIPA buffer (2 mL), homogenized with 5 passes of a homogenizer, and solubilized for 30 minutes at 4°C with shaking. After centrifugation at 12 000*g* for 30 minutes, protein concentrations of supernatants were measured by the BCA protein assay kit (Pierce, Rockford, IL). The supernatants were mixed in Laemmli buffer and boiled. The cell lysates were subjected to SDS–polyacrylamide gel electrophoresis (PAGE) and transferred onto polyvinylidene difluoride membranes (Millipore, Billerica, MA). The membrane was immunoblotted with antibodies to β-actin, DLL4, ephrinB2, or EphB4. The membranes were developed with the enhanced chemiluminescence (ECL) Advance Western Blotting Detection System Plus (Amersham Biosciences, Piscataway, NJ) according to the manufacturer's instructions. Quantification of signals was performed with ImageJ (National Institutes of Health [NIH], Bethesda, MD).

Immunohistochemistry

Immunohistologic staining was performed as described previously.[46] When the diameter of the tumor became approximately 1 cm for HMD4-2 experiments and approximately 1.5 cm for soluble epheinB2 experiments, tumor tissues were fixed in 10% formalin, and embedded in paraffin. Paraffin-embedded sections were cut at 5-μm thickness, deparaffinized, and rehydrated. Endogenous peroxidase activity was blocked with hydrogen peroxide/methanol, and antigen retrieval was performed in a pH 6.0 citrate buffer by autoclave for 5 minutes. After the washing and blocking steps, the resultant tissue sections were incubated overnight with primary antibodies, followed by biotinylated secondary antibodies for 30 minutes at room temperature. Then, immunoreactivity was visualized with an ABC kit (Vector, Burlingame, CA), and detected by 3-amino-9-ethylcarbazole (Vector). The following primary antibodies were used: polyclonal anti–human factor VIII–related antigen antibody (1:200; DAKO), hamster anti–mouse DLL4 antibody (1:5; HMD4-2), and goat anti–mouse ephrinB2 antibody (1;300; R&D Systems). For secondary antibodies, biotinylated

goat anti–mouse IgG antibody (1:200; Vector), goat anti–hamster IgG antibody (1:100; Santa Cruz Biotechnology), and rabbit anti–goat IgG antibody (1:800; Vector) were used.

To measure the hypoxic area, pimonidazole hydrochloride (hypoxyprobe-1; Chemicon) was injected intraperitoneally at a dose of 60 mg/kg 30 minutes before killing, and the vasculature was perfused transcardially with 5 mL of 10% formalin prior to the killing. The distribution of hypoxyprobe-1 was detected using an antihypoxyprobe antibody according to the recommended protocol. The sections were counterstained with hematoxylin.

The intratumoral microvessel area and hypoxic area were quantified. In brief, the intratumoral endothelial cells were stained immunohistochemically with antihuman factor VIII–related antigen antibody, and the hypoxic area was stained with antihypoxyprobe antibody. The images that contained the highest number of endothelial cells were chosen for each section by an initial scan at ×100 magnification. Then the areas of factor VIII–positive cells and those stained with antihypoxyprobe antibody were measured in the selected image at ×100 magnification. At least 4 fields were measured for each section, and the highest count was taken. Two independent investigators evaluated the areas. The sections were photographed with digital camera (Olympus, Melville, NY) attached to an inverted microscope (Nikon, Tokyo, Japan).

Flow cytometry

HUVECs and HMVECs were cultured, treated with trypsin-EDTA, and suspended in PBS. The cells were first incubated with PBS containing 0.1% BSA to block nonspecific binding. After washing, the cells were incubated on ice with a PE-labeled control hamster IgG, PE-labeled control mouse IgG, biotinylated MHD4-46, or biotinylated MHN1-519. The cells were then incubated with PE-conjugated streptavidin (eBioscience, San Diego, CA). After washing again, the cells were subjected to flow cytometry on a FACScan (BD Biosciences, San Jose, CA), and the data were analyzed with CellQuest software (BD Biosciences). For all samples, dead cells were excluded from the analysis by propidium iodide staining.

Cell proliferation assay

The cell proliferation assay was performed as previously described.[46] Briefly, HUVECs (4×10^3/well) or HMVECs (5×10^3/well) were plated onto 96-well plates containing the medium supplemented with MHD4-46 (50 μg/mL), VEGF (100 ng/mL), or control IgG. HUVECs were cultured for 4 days, and the medium was exchanged on day 2. The cell number was determined by water-soluble tetrazolium (WST) assay using a cell counting kit (Dojindo, Kumamoto, Japan).

In vitro angiogenesis (tubular formation) assay

HUVECs and HMVECs were cultured in each culture medium until they were approximately 80% confluent. Before each experiment, the culture medium was replaced with serum-free HuMedia-EB2 (Kurabo) for 16 hours. The cells were then trypsinized, counted, and resuspended at a concentration of 8×10^4 cells/mL in HuMedia-EB2 containing 0.5% FCS and supplemented with rhVEGF (100 ng/mL), MHD4-46 (50 μg/mL), control IgG, or a combination of these. The wells of 24-well tissue culture plates were coated with 0.5 mL/well growth factor–reduced Matrigel (Becton Dickinson Labware, Bedford, MA), which was allowed to solidify at 37.8°C for 30 minutes, according to the manufacturer's instructions. The cell suspensions were then plated (0.5 mL/well) onto the surface of the Matrigel and incubated at 37.8°C. The cells were observed using an inverted phase contrast microscope (Nikon Eclipse TE300) after 12 hours. Images were captured with a laser scanning confocal imaging system (Bio-Rad, Hercules, CA). The length of the cordlike structure and the branch point number were measured in randomly selected fields located within 5 mm of the center of the well using the NIH image program.

In vitro invasion assay

Cell invasion assays were performed using a 96-well BME Cell Invasion Assay (R&D Systems) according to the manufacturer's instructions. This kit was constructed mainly of the 96-well Boyden chamber, 8.0-μm polyester membrane, and the basement membrane extract (BME). In brief, the upper wells of the cell invasion device were coated with the BME, and BMEs were polymerized prior to the addition of cells to the upper wells. HUVECs were starved for 16 hours before the experiment, and seeded onto the upper wells (5×10^4 cells/well) in HuMedia-EB2 without FCS. Lower wells were given HuMedia-EB2 supplemented with VEGF (100 ng/mL), MHD4-46 (50 μg/mL), control IgG, or a combination of these. Twenty-four hours later, HUVECs that had invaded through the ECM to the underside of the membrane were detached from the membranes with the Cell Dissociation Solution, and stained using a Calcein AM (Invitrogen, Tokyo, Japan). The fluorescence was measured by the Fluoroskan Ascent (Labsystems, Arlington, MA). The number of invaded cells was calculated from standard curves.

RNA interference

RNA interference was used to down-regulate the expression of ephrinB2 in HUVECs. Small interference RNA (siRNA) for ephrinB2 (5′-GGAAUAAA-GAUCCAACAAG-3′ or 5′-GGACUGGUACUAUACCCAC-3′) and nonspecific control siRNA (negative control no. 1) were designed and synthesized by Silencer Validated siRNA Design from Ambion (Austin, TX). For gene knockdown experiments, HUVECs were plated in a 10-cm dish, and were transfected with siRNAs (10 nM, control siRNA, siRNA to ephrinB2) using transfection reagent (siPORT NeoFX Transfection Agent; Ambion) according to the manufacturer's instructions.

Data analysis

Statistical analysis of the results was performed using the unpaired Student *t* test for the comparison between 2 sample groups and ANOVA with Fisher least significant difference test for the multiple comparisons. A value of *P* less than .05 was considered significant.

Results

Properties of neutralizing antibodies against mouse and human DLL4

The selective binding of HMD4-2 and MHD4-46 to CHO cells expressing mouse or human DLL4 was confirmed by flow cytometry (Figure 1A). HMD4-2 selectively bound to mouse DLL4, and MHD4-46 selectively bound to human DLL4. We also confirmed the ability of these antibodies to block Notch1-Fc and Notch4-Fc binding to DLL4-expressing CHO cells in a dose-dependent manner (Figure 1B). HMD4-2 blocked the Notch1-Fc and Notch4-Fc binding to mouse DLL4, and MHD4-46 blocked the Notch1-Fc and Notch4-Fc binding to human DLL4. Furthermore, we confirmed that the HMD4-2 did not bind to CHO cells expressing mouse DLL1, Jagged1, or Jagged2 by flow cytometry.[47] Similarly, we confirmed that the MHD4-46 did not bind to CHO cells expressing human DLL1, Jagged1, or Jagged2 by flow cytometry (N.Y. and H.Y., unpublished observation).

DLL4 blockade suppressed tumor growth by inducing nonproductive angiogenesis

To examine the effect of DLL4 blockade on solid tumor growth in vivo, KLN205 cells and LLC cells were implanted subcutaneously in BDF1 or C57BL/6 mice, respectively, and the mice were treated with HMD4-2 or control hamster IgG, as described in "Mouse tumor models." KLN205 tumors showed similar growth rates until day 18 (Figure 1C left). After day 21, the KLN205 tumors treated with HMD4-2 (0.25 mg) were significantly smaller than those treated with control IgG. In the C57BL/6 mice that received an implant of LLC cells, we treated mice with 2 different doses of HMD4-2 (Figure 1C right). Tumors of the

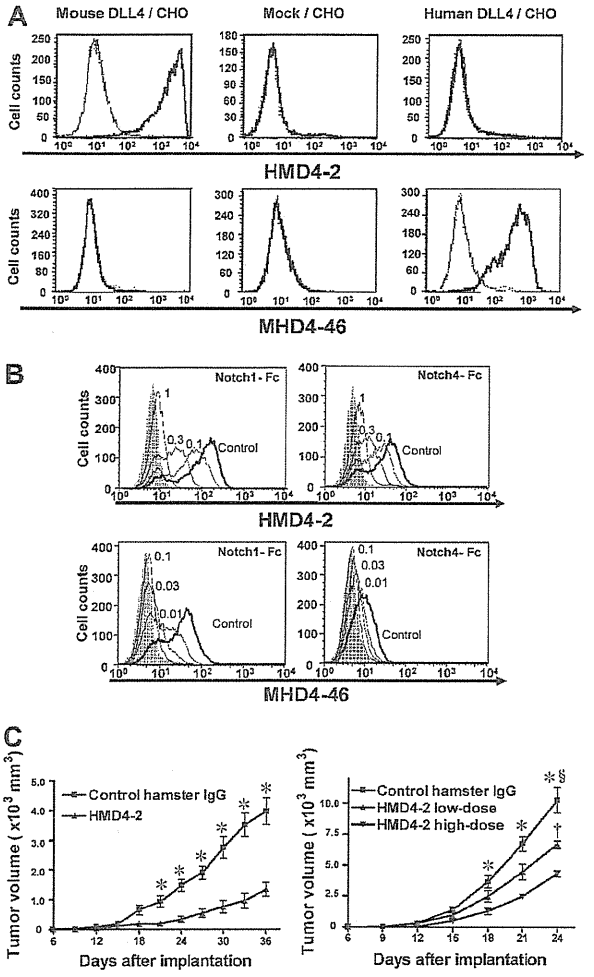

Figure 1. Characterization of HMD4-2 and MHD4-46 and effect of HMD4-2 on tumor growth. (A) Flow cytometric analysis showed the specific bindings of HMD4-2 to mouse DLL4 and MHD4-46 to human DLL4. Bold histogram shows the staining with biotinylated HMD4-2 or MHD4-46 followed by PE-labeled streptavidin. Thin histogram shows the staining with biotinylated control hamster IgG or control mouse IgG1 followed by PE-labeled streptavidin. (B) The antibodies blocked Notch1-Fc and Notch4-Fc binding to DLL4. Binding of mouse Notch1-Fc (top left) and mouse Notch4-Fc (top right) to mouse Dll4/CHO cells was blocked by the indicated doses (μg) of HMD4-2. Binding of human Notch1-Fc (bottom left) and mouse Notch4-Fc (bottom right) to human Dll4/CHO cells was blocked by the indicated doses (μg) of MHD4-46. The shaded histograms indicate the background staining without Notch-Fc. (C) HMD4-2 inhibited subcutaneous tumor growth in mouse tumor models with KLN205 (left) and LLC (right). The vertical axis showed the tumor volume and horizontal axis showed the time after implantation. The values represent the mean plus or minus SE (n = 7-10 per group). $^*P < .05$ versus control, §$P < .05$ versus HMD4-2 low dose, †$P < .05$ versus HMD4-2 high dose, by Student unpaired *t* test or 1-way ANOVA with Fisher least-significant-difference test at each time point.

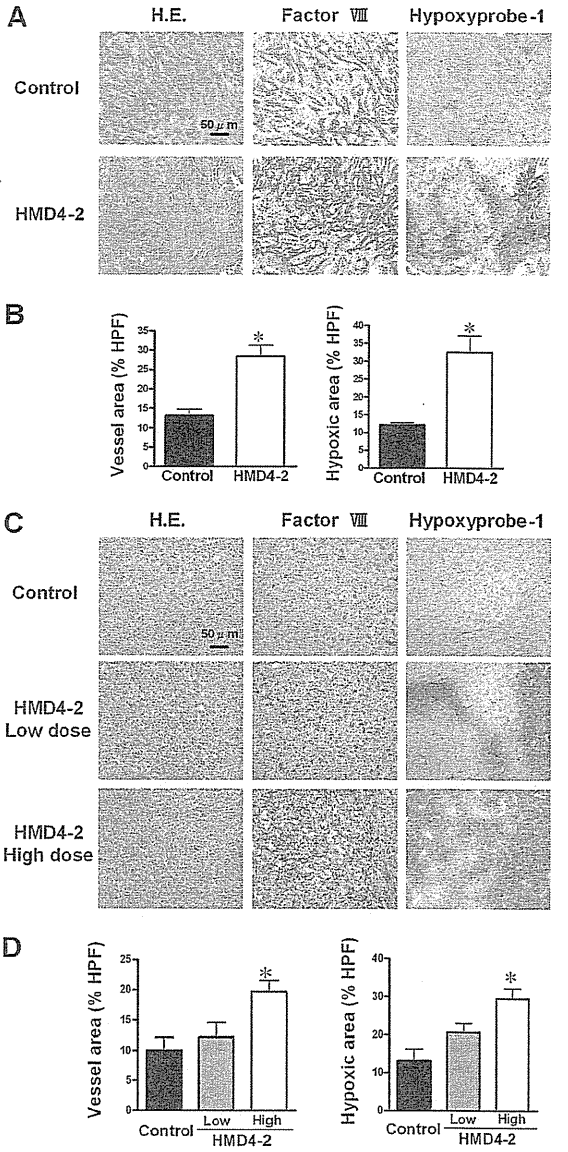

Figure 2. Effect of HMD4-2 on tumor angiogenesis and hypoxia. (A,C) Hematoxylin and eosin (H.E.) staining and immunohistologic staining for factor VIII–related antigen and for hypoxia (hypoxyprobe-1 kit) of KLN205 tumors (A) and LLC tumors (C). The hypoxic area was stained brown. (B,D) The quantitative analyses of histologic data of KLN205 tumors (B) and LLC tumors (D). The factor VIII–positive vessel area and hypoxic area were measured, and the percentages of the area in HPF (×100) were compared in each mouse tumor model. Data are mean plus or minus SE (n = 7 per group). $^*P < .05$ versus control by Student unpaired *t* test or 1-way ANOVA with Fisher least-significant-difference test.

high-dose HMD4-2 (1 mg) group were significantly smaller than those of the control group after day 18. Tumors of the low-dose HMD4-2 (0.25 mg) group were significantly smaller than those of the control group and were significantly larger than tumors of the high-dose HMD4-2 group at day 24.

To evaluate angiogenesis and hypoxic lesions in these tumors, we immunostained the sections for factor VIII, which is expressed on endothelial cells, and used a hypoxyprobe-1 kit to detect hypoxic lesions. The immunostaining showed a significant increase of factor VIII–positive endothelial cells in tumors treated with HMD4-2 (Figure 2A-D). However, hypoxic lesions were also significantly increased in HMD4-2–treated mice (Figure 2A-D). Moreover, these effects were dose dependent in LLC groups (Figure 2C,D). These results suggested that the suppressive effect of HMD4-2 on tumor growth was caused by the increased nonfunctional angiogenesis resulting in a reduced blood supply represented as an increase of hypoxic area in tumors.

DLL4 was expressed in KLN205 tumors and DLL4 blockade suppressed ephrinB2 expression

In vitro cultured KLN205 cells and LLC cells did not express DLL4 as estimated by reverse-transcription (RT)–PCR, Western blotting, or flow cytometry (data not shown). Therefore, whether DLL4 was expressed in

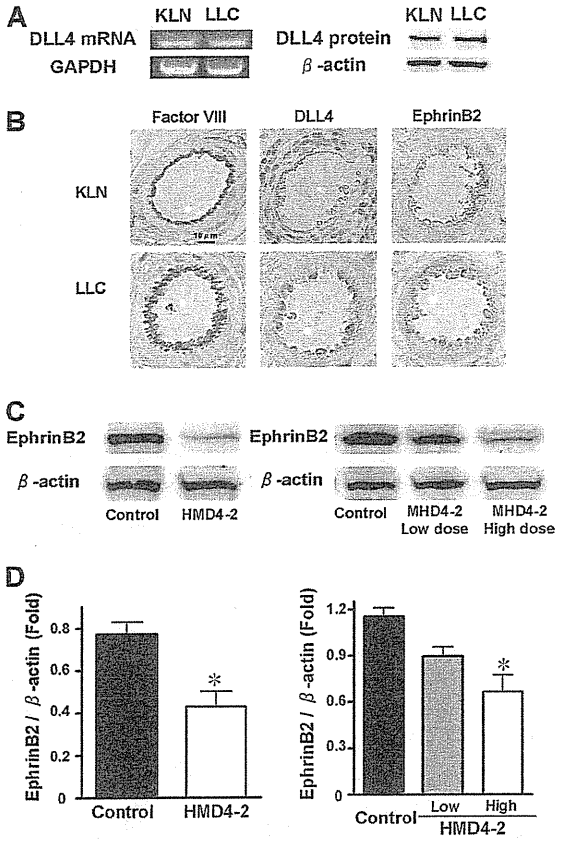

Figure 3. Expression of DLL4 and ephrinB2 in KLN205 and LLC tumors. (A) Expression of DLL4 in subcutaneous KLN205 and LLC tumors was detected by RT-PCR (left) and Western blotting (right). (B) Representative immunohistochemical staining of factor VIII–related antigen, DLL4, and ephrinB2. Data were obtained from serial sections of the same area in both KLN205 and LLC tumors. (C) Western blotting of ephrinB2 in KLN205 (left) and LLC (right) tumors. (D) The relative expression of ephrinB2 was measured by densitometric analysis in KLN205 tumors (left) and LLC tumors (right). The results are expressed as the ratio of the amount of ephrinB2 protein to the amount of β-actin. Data are mean plus or minus SE (n = 7 per group). *$P < .05$ versus control by Student unpaired t test (left) or 1-way ANOVA with Fisher least-significant-difference test (right).

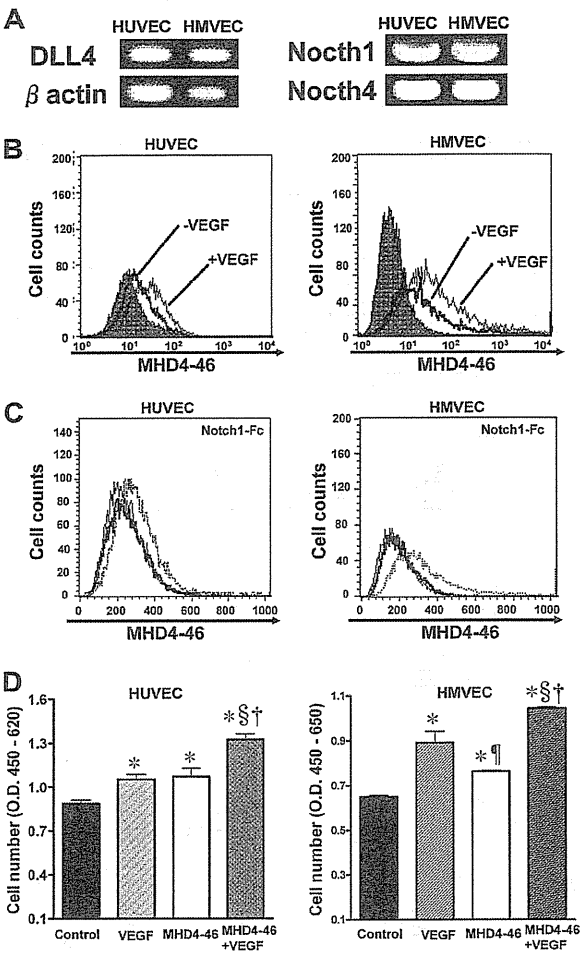

Figure 4. DLL4 blockade facilitated proliferation of HUVECs in vitro. (A) Expression of DLL4, Notch1, and Notch4 in HUVECs and HMVECs was examined by RT-PCR. (B) The change of DLL4 expression was examined before or after VEGF stimulation by flow cytometry. The gray histogram shows the background staining with control mouse IgG1. (C) The dotted histogram shows the binding of Notch1-Fc after preincubation of the indicated cells with control IgG. The bold histogram shows the binding of Notch1-Fc after preincubation of the indicated cells with MHD4-46. Thin histogram shows the background staining. (D) HUVECs and HMVECs were treated with VEGF, MHD4-46, or both, and proliferation was determined by WST assay. The values represent mean plus or minus SE of triplicate wells repeated twice. *$P < .05$ versus control, ¶ and §$P < .05$ versus VEGF, †$P < .05$ versus MHD4-46 by 1-way ANOVA with Fisher least-significant-difference test.

the KLN205 and LLC tumor tissues was investigated. KLN205 and LLC tumors were isolated, and homogenized to extract mRNAs and proteins. In both KLN205 and LLC tumors, DLL4 was detected at comparable levels by both Western blotting and RT-PCR (Figure 3A). Immunohistochemical staining of KLN205 and LLC tumors showed that both DLL4 and ephrinB2 were expressed in the vascular endothelium in relatively larger vessels where cells were positively stained by factor VIII–related antigen antibody (Figure 3B). We further investigated ephrinB2 expression in HMD4-2–treated tumors. Western blotting showed that the expression of ephrinB2 was significantly decreased in the HMD4-2–treated tumors in comparison with those treated with control IgG in both KLN205 and LLC tumors, and these effects were dose dependent (Figure 3C,D). EphB4 expression in these tumors was not influenced by HMD4-2 treatments (data not shown).

DLL4 blockade promoted proliferation of endothelial cells

We found that HUVECs and HMVECs expressed DLL4, Notch1, and Notch4 as estimated by RT-PCR and flow cytometry for DLL4 with MHD4-46 (Figure 4A,B). VEGF (100 ng/mL) stimulation increased the DLL4 expression as estimated by flow cytometry (Figure 4B bottom). We confirmed the ability of MHD4-46 to block Notch1-Fc binding to DLL4 on HUVECs and HMVECs (Figure 4C). Then, the effect of DLL4 blockade on proliferation of these cell lines using MHD4-46 was investigated. MHD4-46 significantly promoted proliferation of these cell lines, and this proliferative effect was comparable with that of VEGF in HUVECs (Figure 4D). Notably, the proliferative effects of MHD4-46 and VEGF were additive.

Effect of DLL4 blockade on in vitro tubular formation and invasion

Tubular formation and invasion assays were performed to investigate the interaction between MHD4-46 and VEGF in in vitro angiogenesis. Tubular formations of HUVECs and HMVECs were affected by the addition of VEGF and/or MHD4-46 (Figure 5A). As shown in Figure 5B, either VEGF or MHD4-46 significantly increased cord length in the tubular formation assay. However, the

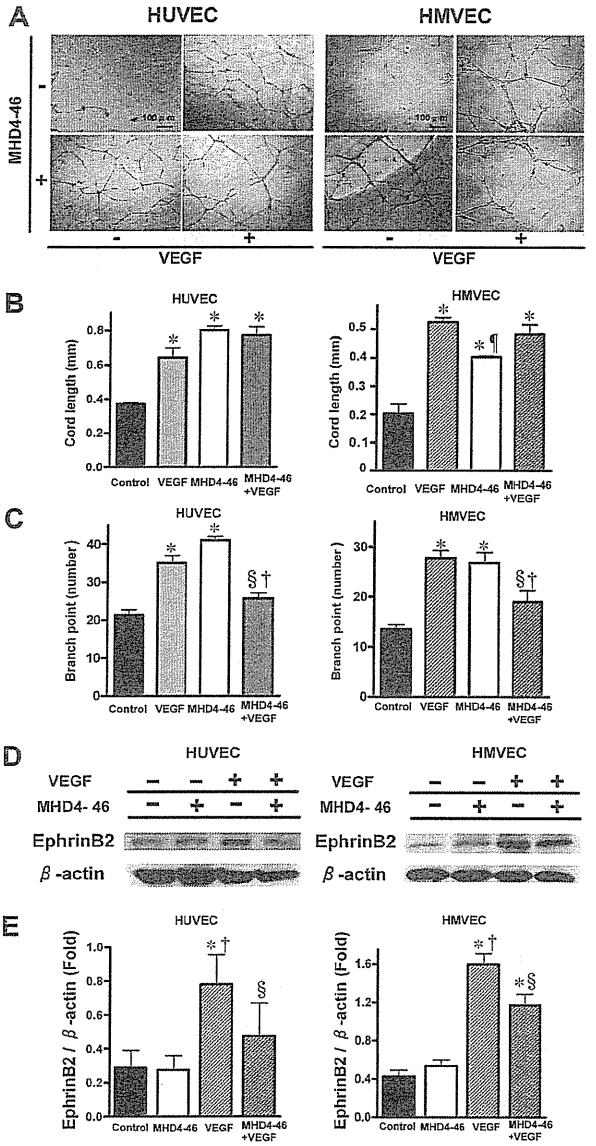

Figure 5. DLL4 blockade increased cord length, but decreased branch point number and suppressed VEGF-induced ephrinB2 expression. (A) Effect of MHD4-46 on HUVEC and HMEVC tubular formation. Representative microphotographs at ×100 magnification from triplicate wells of experiments repeated twice are shown. (B,C) Quantitative data of cord length (B) and brunch point number (C). (D) Protein expression of ephrinB2 and β-action in HUVECs and HMVECs. (E) The relative expression of ephrinB2 to β-action was measured by densitometric analysis. Data are shown as mean plus or minus SE of triplicate wells from the representative result of 3 independent experiments. *$P < .05$ versus control, §$P < .05$ versus VEGF, †$P < .05$ versus MHD4-46 by 1-way ANOVA with Fisher least-significant-difference test.

combination of MHD4-46 and VEGF did not show an additive effect in cord length (Figure 5B). As shown in Figure 5C, both MHD4-46 and VEGF significantly increased the branch point number. In contrast, the branch point number in the combined application of MHD4-46 and VEGF was the same as the control and significantly lower than VEGF or MHD4-46 alone, suggesting that the effects of VEGF and MHD4-46 could counteract each other (Figure 5C). We also performed a cell invasion assay using the Boyden chamber. MHD4-46 itself did not induce the cell invasion. In addition, MHD4-46 had no apparent effect on VEGF-induced invasion of these cell lines (data not shown).

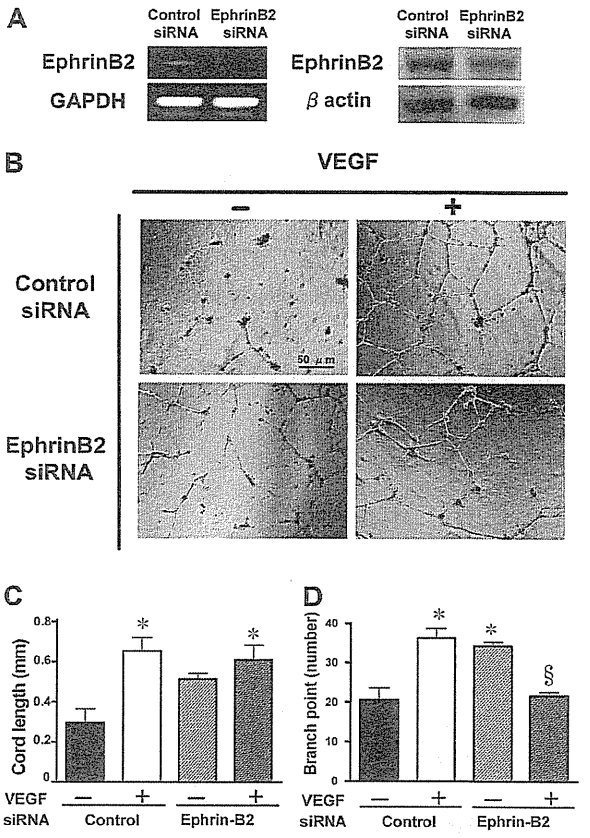

Figure 6. Knockdown of ephrinB2 with siRNA and its effects on in vitro tubular formation. (A) Knockdown of ephrinB2 in HUVECs was evaluated both at mRNA and protein levels. The reduction rates in fold expression (ephrinB2 siRNA/control siRNA) of mRNA and protein levels were approximately 27% and 60%, respectively. (B) Effect of ephrinB2 knockdown on HUVEC tubular formation. Representative microphotographs at ×100 magnification from triplicate wells of 2 repeated experiments are shown. Quantitative data of cord length (C) and branch point number (D). Data are shown as mean plus or minus SE of triplicate wells in 2 experiments. *$P < .05$ versus control siRNA without VEGF and §$P < .05$ versus control siRNA with VEGF by 1-way ANOVA with Fisher least-significant-difference test.

DLL4 blockade suppressed VEGF-induced ephrinB2 expression in endothelial cells

Since we found that the ephrinB2 expression in both KLN205 and LLC tumors was reduced by the DLL4 blockade in vivo, we hypothesized that this reduction occurred in the endothelial cells in tumor blood vessels. Therefore, we investigated the effect of DLL4 blockade on VEGF-induced ephrinB2 expression in HUVECs and HMVECs (Figure 5D,E). VEGF alone significantly enhanced the ephrinB2 expression in these endothelial cell lines, whereas MHD4-46 alone did not. The VEGF-induced enhancement of ephrinB2 was significantly inhibited by the addition of MHD4-46 (Figure 5E), suggesting that VEGF-induced ephrinB2 expression was mediated by DLL4 in endothelial cells.

Knockdown of ephrinB2 mimicked the effect of DLL4 blockade

To investigate whether the DLL4-induced nonproductive angiogenesis resulted from suppression of ephrinB2, we performed an in vitro tubular formation assay after knockdown of ephrinB2 by RNA interference. Following 24 hours of transfection, a significant reduction of both mRNA and protein levels was achieved (Figure 6A). These HUVECs were plated on matrigel-coated wells, and

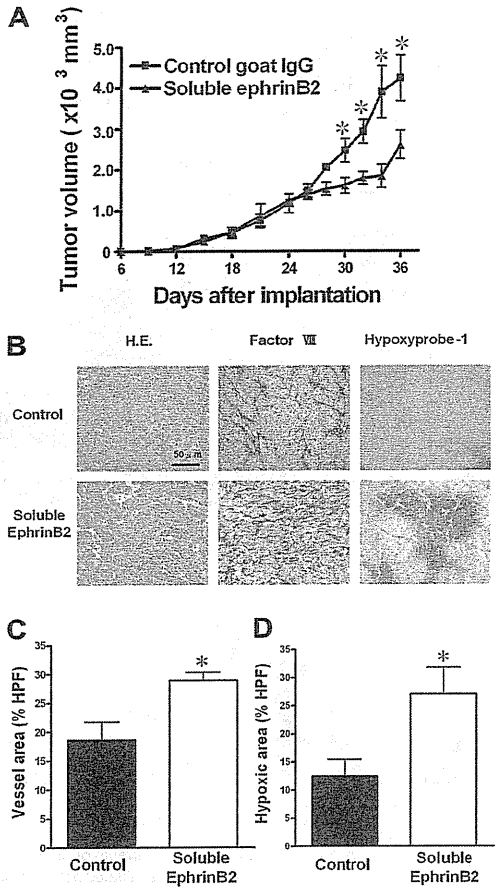

Figure 7. Effect of soluble ephrinB2 on tumor growth. (A) A soluble form of ephrinB2 (ephrinB2-Fc) inhibited subcutaneous tumor growth in a mouse tumor models with KLN205. (B) Hematoxylin and eosin (H.E.) staining and immunohistologic staining for factor VIII–related antigen and for hypoxia (hypoxyprobe-1 kit). (C,D) The quantitative analyses of histologic data. The factor VIII–positive vessel area (C) and hypoxic area (D) were measured, and the percentages of the area in HPF (×100) were compared. Data are mean plus or minus SE (n = 7 per group). *$P < .05$ versus control by Student unpaired t test.

stimulated with VEGF for 12 hours (Figure 6B). Although the knockdown of ephrinB2 alone did not significantly increase the cord length, it significantly increased the branch point number (Figure 6D). In the presence of VEGF in the tubular formation, knockdown of ephrinB2 significantly inhibited VEGF-induced enhancement of the branch point number but not the cord length (Figure 6C,D). We confirmed this effect using 2 different siRNAs as described in "RNA interference."

Soluble form of ephrinB2 induced nonproductive angiogenesis and suppressed tumor growth

We investigated the effect of ephrinB2 interference on in vivo solid tumor growth using a soluble form of ephrinB2, recombinant mouse ephrinB2-Fc, as described in "Mouse tumor models." Intratumoral injection of ephrinB2-Fc significantly suppressed KLN205 tumor growth compared with control IgG (Figure 7A). Histologic analysis revealed a significant increase in factor VIII–related antigen-positive vessels and hypoxic area when treated with ephrinB2-Fc, indicating angiogenesis (Figure 7B-D). These results suggested that ephrinB2/EphB signaling plays an important role in nonproductive angiogenesis.

Discussion

In this study, we showed that the blockade of DLL4 by HMD4-2 inhibited tumor growth accompanied by nonproductive angiogenesis and decreased ephrinB2 expression in tumor tissues. In addition, knockdown of ephrinB2 mimicked the effect of DLL4 on the HUVEC tubular formation. Moreover, we found that the interference of ephrinB2/Eph signaling induced nonproductive angiogenesis in tumors. These results suggest the decrease in ephrinB2 by DLL4 blockade was involved in the nonproductive angiogenesis.

A similar antitumor effect of DLL4 blockade was recently reported and characterized by nonproductive angiogenesis.[41,43] In this abnormal angiogenesis, thin, dense, and nonperfusing vessels with few pericytes were observed.[42] In our study, we also observed the same phenomena. It was also previously reported that VEGF induced the expression of DLL4 in vivo and in vitro[38,39] and that DLL4 stimulation markedly induced ephrinB2 on endothelial cells in vitro.[37] Another group reported the VEGF-DLL4-ephrinB2 cascade played a key role in the remodeling of tumor vessels.[26] However, it has not been elucidated whether this cascade was involved in the nonproductive angiogenesis.

Up-regulation of ephrinB2 signaling enlarges vessel size and decreases vessel density in mouse tumor models.[33-35] These effects of ephrinB2 signaling seemed to be opposite to those of DLL4 blockade. Moreover, ephrinB2 and its receptor EphB4 were critical for recruitment of mural cells and assembly of the vessel wall.[32,48,49] Therefore, we investigated the ephrinB2 expression in this nonproductive angiogenesis, and confirmed the decrease in ephrinB2 expression in the tumors treated with HMD4-2. In vitro, the blockade of DLL4 with MHD4-46 promoted HUVEC proliferation and increased cord length and branch point number in the in vitro tubular formation assay. These data may explain the in vivo data such as the increased number and dense network of endothelial cells in the tumors. However, the combination of VEGF and MHD4-46 had no additive effect on cord length and diminished the facilitating effect on branch point number, suggesting the existence of cross-talk in the intracellular signaling pathways of vascular differentiations between VEGF and DLL4 in endothelial cells. The differences in vivo and in vitro may be explained by differences in the environment around endothelial cells, since tumor angiogenesis was performed not only by endothelial cells but also by various surrounding cells such as cancer cells, mural cells, pericytes, and macrophages.

We also investigated the relationship between DLL4 blockade and ephrinB2 expression in HUVECs in vitro. HUVECs have weak basal ephrinB2 expression, and this expression was enhanced by the addition of VEGF (Figure 5). MHD4-46 blocked this cascade and inhibited the VEGF-induced ephrinB2 expression. Although the other pathways were also implicated, these results suggest that VEGF-induced ephrinB2 expression was mediated, at least in a part, by DLL4. Knockdown of ephrinB2 resulted in an increase in branch point number, but did not affect cord length in the presence of VEGF. Since knockdown of ephrinB2 mimicked the effect of MHD4-46 on VEGF-induced endothelial differentiation, this suggests that DLL4 blockade induced the abnormal angiogenesis through the ephrinB2 suppression.

The soluble form of ephrinB2 is known to perturb ephrinB2/Eph signaling.[50-52] In HUVECs, soluble ephrinB2 suppressed VEGF-induced ERK1/2 phosphorylation and Ras activation, resulting in inhibition of VEGF-induced endothelium proliferation,

sprouting, and migration.[53] In HMVECs, soluble ephrinB2 inhibited VEGF-induced migration by direct activation of the kinase activity of EphB4.[50] In a mouse model of proliferative retinopathy, soluble ephrinB2 reduced retinal neovascularization.[51] In our in vivo experiments, soluble ephrinB2 inhibited tumor growth and induced nonproductive angiogenesis (Figure 7). Moreover, we found that DLL4 blockade inhibited ephrinB2 in a dose-dependent manner, and induced nonproductive angiogenesis also in a dose-dependent manner in LLC tumors (Figures 1C, 2, and 3C,D). Taken together, involvement of ephrinB2 is implied as an underlying mechanism of nonproductive angiogenesis induced by DLL4 blockade.

Eph/ephrin pathways appear to be essential for morphogenesis of various organs in the embryo, because they regulate many of the dynamic changes that occur during this embryonic stage, including cell migration, axon guidance, and angiogenesis.[27] Mutant animals lacking ephrinB2 die before day 11 of embryonic development, displaying defects in angiogenic remodeling.[30,31] Eph and ephrin molecules are up-regulated not only in the embryonic stage but also in cancers and may affect tumor growth and neovascularization.[26,33-35]

In regard to ephrinB2, recent studies showed that EphB4/ephrinB2 interaction inhibited endothelial sprouting and promoted circumferential growth of vessels, and another group reported reverse signaling via ephrinB2 induced low microvascular density but large vessel diameter resulting in tumor progression.[33-35] The ephrinB2 function in tumor angiogenesis seems to be quite contrary to that of DLL4 blockade. Here, we demonstrated DLL4 blockade induced nonproductive angiogenesis, at least in part, through ephrinB2 suppression. We do not consider ephrinB2 as the only target of DLL4, because DLL4 or VEGF is the gene whose haploinsufficiency led to embryonic lethality, whereas ephrinB2 is not.[21] Our data suggest that a decrease in ephrinB2 expression played, at least in part, an important role in the nonproductive angiogenesis induced by DLL4 blockade.

Solid tumors require blood vessels for growth. Therefore, antiangiogenic therapies have emerged as an important option for treating several types of cancers.[1] It was considered that antiangiogenic therapy killed cancer cells by depriving oxygen and nutrients, so that it could reduce drug delivery and induce hypoxia-related resistance to chemotherapy and radiotherapy.[52] However, the combination of anti-VEGF agents with cytotoxic drugs or irradiation showed promising results in many clinical and basic studies.[3,52] To resolve this paradox, it was proposed that an antiangiogenic agent could transiently "normalize" the abnormal tumor vasculature, resulting in more efficient delivery of oxygen and drugs, and many reports support this hypothesis.[49] However, the nonproductive angiogenesis induced by DLL4 blockade showed little perfusion of blood and hypoxia.[41-44] It was opposed to "normalization," but significantly inhibited tumor growth. Therefore, DLL4 blockade might cause more severe and sustained hypoxia than anti-VEGF therapy.

DLL4 blockade could be effective for tumors resistant to anti-VEGF therapy.[41] It is conceivable that the target of DLL4 blockade in tumor angiogenesis was to inhibit tumor vascular remodeling or maturation, whereas that of anti-VEGF therapy was to switch off the trigger of tumor angiogenesis. Therefore, DLL4 blockade would be effective for tumors that do not respond to anti-VEGF therapy.

In our experiments, we showed the antitumor effect of DLL4 blockade using newly developed neutralizing antibodies against DLL4, and demonstrated the VEGF-DLL4-ephrinB2 cascade could be involved in the nonproductive angiogenesis induced by DLL4 blockade. The effect of DLL4 blockade on tumor angiogenesis seems to be different from that of anti-VEGF therapy, and this difference could provide us a new option for the therapeutic strategy for cancer treatment.

Acknowledgment

This study was supported by a Grant-In-Aid for Scientific Research from the Ministry of Education, Science and Culture of the Japanese government to M.A. (no. 19790553) and to S.E. (nos. 18014004, 19590688).

Authorship

Contribution: S.Y. and S.E. designed and performed research, analyzed data, and wrote the paper; M.A., T.O., and T.E. performed research and analyzed data; K.N. performed research; A.K. and N.Y. contributed vital new reagents and analyzed data; H.Y. organized analysis, contributed vital new reagents, and wrote the paper; and H.A. designed research and wrote the paper.

Conflict-of-interest disclosure: The authors declare no competing financial interests.

Correspondence: Satoru Ebihara, Department of Geriatrics and Gerontology, Institute of Development, Aging and Cancer, Tohoku University, Seiryo-machi 4-1, Aoba-ku, Sendai, 980-8575, Japan; e-mail: sebihara@idac.tohoku.ac.jp.

References

1. Folkman J. Tumor angiogenesis: therapeutic implications. N Engl J Med. 1971;285:1182-1186.
2. Ferrara N, Alitalo K. Clinical applications of angiogenic growth factors and their inhibitors. Nat Med. 1999;5:1359-1364.
3. Jain RK, Duda DG, Clark JW, Loeffler JS. Lessons from phase III clinical trials on anti-VEGF therapy for cancer. Nat Clin Pract Oncol. 2006;3:24-40.
4. Artavanis-Tsakonas S, Rand MD, Lake RJ. Notch signaling: cell fate control and signal integration in development. Science. 1999;284:770-776.
5. Mumm JS, Kopan R. Notch signaling: from the outside in. Dev Biol. 2000;228:151-165.
6. Weinmaster G. Notch signaling: direct or what? Curr Opin Genet Dev. 1998;8:436-442.
7. Davis RL, Turner DL. Vertebrate hairy and Enhancer of split related proteins: transcriptional repressors regulating cellular differentiation and embryonic patterning. Oncogene. 2001;20:8342-8357.
8. Iso T, Kedes L, Hamamori Y. HES and HERP families: multiple effectors of the Notch signaling pathway. J Cell Physiol. 2003;194:237-255.
9. Nakagawa O, McFadden DG, Nakagawa M, et al. Members of the HRT family of basic helix-loop-helix proteins act as transcriptional repressors downstream of Notch signaling. Proc Natl Acad Sci U S A. 2000;97:13655-13660.
10. Lawson ND, Weinstein BM. Arteries and veins: making a difference with zebrafish. Nat Rev Genet. 2002;3:674-682.
11. Rossant J, Howard L. Signaling pathways in vascular development. Annu Rev Cell Dev Biol. 2002;18:541-573.
12. Shawber CJ, Kitajewski J. Notch function in the vasculature: insights from zebrafish, mouse and man. Bioessays. 2004;26:225-234.
13. Herreman A, Hartmann D, Annaert W, et al. Presenilin 2 deficiency causes a mild pulmonary phenotype and no changes in amyloid precursor protein processing but enhances the embryonic lethal phenotype of presenilin 1 deficiency. Proc Natl Acad Sci U S A. 1999;96:11872-11877.
14. Krebs LT, Xue Y, Norton CR, et al. Notch signaling is essential for vascular morphogenesis in mice. Genes Dev. 2000;14:1343-1352.
15. Xue Y, Gao X, Lindsell CE, et al. Embryonic lethality and vascular defects in mice lacking the Notch ligand Jagged1. Hum Mol Genet. 1999;8:723-730.
16. Uyttendaele H, Ho J, Rossant J, Kitajewski J.

Vascular patterning defects associated with expression of activated Notch4 in embryonic endothelium. Proc Natl Acad Sci U S A. 2001;98:5643-5648.

17. Shawber CJ, Das I, Francisco E, Kitajewski J. Notch signaling in primary endothelial cells. Ann N Y Acad Sci. 2003;995:162-170.
18. Shutter JR, Scully S, Fan W, et al. Dll4, a novel Notch ligand expressed in arterial endothelium. Genes Dev. 2000;14:1313-1318.
19. Duarte A, Hirashima M, Benedito R, et al. Dosage-sensitive requirement for mouse Dll4 in artery development. Genes Dev. 2004;18:2474-2478.
20. Krebs LT, Shutter JR, Tanigaki K, Honjo T, Stark KL, Gridley T. Haploinsufficient lethality and formation of arteriovenous malformations in Notch pathway mutants. Genes Dev. 2004;18:2469-2473.
21. Ferrara N, Carver-Moore K, Chen H, et al. Heterozygous embryonic lethality induced by targeted inactivation of the VEGF gene. Nature. 1996;380:439-442.
22. Mailhos C, Modlich U, Lewis J, Harris A, Bicknell R, Ish-Horowicz D. Delta4, an endothelial specific notch ligand expressed at sites of physiological and tumor angiogenesis. Differentiation. 2001;69:135-144.
23. Patel NS, Dobbie MS, Rochester M, et al. Up-regulation of endothelial delta-like 4 expression correlates with vessel maturation in bladder cancer. Clin Cancer Res. 2006;12:4836-4844.
24. Shi W, Harris AL. Notch signaling in breast cancer and tumor angiogenesis: cross-talk and therapeutic potentials. J Mammary Gland Biol Neoplasia. 2006;11:41-52.
25. Buchler P, Gazdhar A, Schubert M, et al. The Notch signaling pathway is related to neurovascular progression of pancreatic cancer. Ann Surg. 2005;242:791-800, discussion 800-801.
26. Hainaud P, Contreres JO, Villemain A, et al. The role of the vascular endothelial growth factor-Delta-like 4 ligand/Notch4-Ephrin B2 cascade in tumor vessel remodeling and endothelial cell functions. Cancer Res. 2006;66:8501-8510.
27. Pasquale EB. Eph receptor signalling casts a wide net on cell behaviour. Nat Rev Mol Cell Biol. 2005;6:462-475.
28. Gale NW, Holland SJ, Valenzuela DM, et al. Eph receptors and ligands comprise two major specificity subclasses and are reciprocally compartmentalized during embryogenesis. Neuron. 1996;17:9-19.
29. Cheng N, Brantley DM, Chen J. The ephrins and Eph receptors in angiogenesis. Cytokine Growth Factor Rev. 2002;13:75-85.
30. Adams RH, Diella F, Hennig S, Helmbacher F, Deutsch U, Klein R. The cytoplasmic domain of the ligand ephrinB2 is required for vascular morphogenesis but not cranial neural crest migration. Cell. 2001;104:57-69.
31. Wang HU, Chen ZF, Anderson DJ. Molecular distinction and angiogenic interaction between embryonic arteries and veins revealed by ephrin-B2 and its receptor Eph-B4. Cell. 1998;93:741-753.
32. Adams RH, Wilkinson GA, Weiss C, et al. Roles of ephrinB ligands and EphB receptors in cardiovascular development: demarcation of arterial/venous domains, vascular morphogenesis, and sprouting angiogenesis. Genes Dev. 1999;13:295-306.
33. Erber R, Eichelsbacher U, Powajbo V, et al. EphB4 controls blood vascular morphogenesis during postnatal angiogenesis. EMBO J. 2006;25:628-641.
34. Noren NK, Foos G, Hauser CA, Pasquale EB. The EphB4 receptor suppresses breast cancer cell tumorigenicity through an Abl-Crk pathway. Nat Cell Biol. 2006;8:815-825.
35. Noren NK, Lu M, Freeman AL, Koolpe M, Pasquale EB. Interplay between EphB4 on tumor cells and vascular ephrin-B2 regulates tumor growth. Proc Natl Acad Sci U S A. 2004;101:5583-5588.
36. Harrington LS, Sainson RC, Williams CK, et al. Regulation of multiple angiogenic pathways by Dll4 and Notch in human umbilical vein endothelial cells. Microvasc Res. 2008;75:144-154.
37. Iso T, Maeno T, Oike Y, et al. Dll4-selective Notch signaling induces ephrinB2 gene expression in endothelial cells. Biochem Biophys Res Commun. 2006;341:708-714.
38. Liu ZJ, Shirakawa T, Li Y, et al. Regulation of Notch1 and Dll4 by vascular endothelial growth factor in arterial endothelial cells: implications for modulating arteriogenesis and angiogenesis. Mol Cell Biol. 2003;23:14-25.
39. Lobov IB, Renard RA, Papadopoulos N, et al. Delta-like ligand 4 (Dll4) is induced by VEGF as a negative regulator of angiogenic sprouting. Proc Natl Acad Sci U S A. 2007;104:3219-3224.
40. Suchting S, Freitas C, le Noble F, et al. The Notch ligand Delta-like 4 negatively regulates endothelial tip cell formation and vessel branching. Proc Natl Acad Sci U S A. 2007;104:3225-3230.
41. Noguera-Troise I, Daly C, Papadopoulos NJ, et al. Blockade of Dll4 inhibits tumour growth by promoting non-productive angiogenesis. Nature. 2006;444:1032-1037.
42. Scehnet JS, Jiang W, Kumar SR, et al. Inhibition of Dll4-mediated signaling induces proliferation of immature vessels and results in poor tissue perfusion. Blood. 2007;109:4753-4760.
43. Ridgway J, Zhang G, Wu Y, et al. Inhibition of Dll4 signalling inhibits tumour growth by deregulating angiogenesis. Nature. 2006;444:1083-1087.
44. Thurston G, Noguera-Troise I, Yancopoulos GD. The Delta paradox: DLL4 blockade leads to more tumour vessels but less tumour growth. Nat Rev Cancer. 2007;7:327-331.
45. National Research Council. Guide for the Care and Use of Laboratory Animals. Washington, DC: National Academy Press; 1985. NIH publication no. 86-23.
46. Okazaki T, Ebihara S, Takahashi H, Asada M, Kanda A, Sasaki H. Macrophage colony-stimulating factor induces vascular endothelial growth factor production in skeletal muscle and promotes tumor angiogenesis. J Immunol. 2005;174:7531-7538.
47. Moriyama Y, Sekine C, Koyanagi A, et al. Delta-like 1 is essential for the maintenance of marginal zone B cells in normal mice but not autoimmune mice. Int Immunol. 2008;20:763-773.
48. Shin D, Garcia-Cardena G, Hayashi S, et al. Expression of ephrinB2 identifies a stable genetic difference between arterial and venous vascular smooth muscle as well as endothelial cells, and marks subsets of microvessels at sites of adult neovascularization. Dev Biol. 2001;230:139-150.
49. Foo SS, Turner CJ, Adams S, et al. Ephrin-B2 controls cell motility and adhesion during blood-vessel-wall assembly. Cell. 2006;124:161-173.
50. Sturz A, Bader B, Thierauch KH, Glienke J. EphB4 signaling is capable of mediating ephrinB2-induced inhibition of cell migration. Biochem Biophys Res Commun. 2004;313:80-88.
51. Zamora DO, Davies MH, Plank SR, Rosenbaum JT, Powers MR. Soluble forms of ephrinB2 and EphB4 reduce retinal neovascularization in a model of proliferative retinopathy. Invest Ophthalmol Vis Sci. 2005;46:2175-2182.
52. Jain RK. Normalization of tumor vasculature: an emerging concept in antiangiogenic therapy. Science. 2005;307:58-62.
53. Kim I, Ryu YS, Kwak HJ, et al. EphB ligand, ephrinB2, suppresses the VEGF- and angiopoietin 1-induced Ras/mitogen-activated protein kinase pathway in venous endothelial cells. FASEB J. 2002;16:1126-1128.

NEOPLASIA
www.neoplasia.com

Volume 11 Number 4 April 2009 pp. 408–417 408

Depletion of Serotonin and Selective Inhibition of 2B Receptor Suppressed Tumor Angiogenesis by Inhibiting Endothelial Nitric Oxide Synthase and Extracellular Signal–Regulated Kinase 1/2 Phosphorylation[1,2]

Masanori Asada*, Satoru Ebihara*, Shinsuke Yamanda*, Kaijun Niu*, Tatsuma Okazaki*, Ichiro Sora† and Hiroyuki Arai*

*Department of Geriatrics and Gerontology, Institute of Development, Aging and Cancer, Tohoku University, Seiryo-machi 4-1, Aoba-ku, Sendai 980-8575, Japan; †Department of Psychobiology, Tohoku University Graduate School of Medicine, Seiryo-machi 1-1, Aoba-ku, Sendai 980-8574, Japan

Abstract

The effects of serotonin (5-HT) on tumor growth are inconsistent. We investigated whether a decreased level of 5-HT affected tumor growth using 5-HT transporter knockout (*5-HTT*$^{-/-}$) mice, which showed 5-HT depletion. When cancer cells were injected subcutaneously into both *5-HTT*$^{-/-}$ and *5-HTT*$^{+/+}$ mice, the tumor growth was markedly attenuated in *5-HTT*$^{-/-}$ mice. Serotonin levels in the blood, forebrain, and tumors of *5-HTT*$^{-/-}$ mice bearing tumors were significantly smaller than those of their *5-HTT*$^{+/+}$ littermates. However, 5-HT did not increase cancer cells' proliferation *in vitro*. When we applied 5-HTT inhibitors to the wild mice bearing tumors, they did not inhibit tumor growth. The endothelial nitric oxide synthase (eNOS) expressions in tumors were reduced in *5-HTT*$^{-/-}$ mice compared with *5-HTT*$^{+/+}$ mice. Stimulations with 5-HT (1-50 μM) induced eNOS expressions in human umbilical vein endothelial cell (HUVEC) in a concentration-dependent manner. When we measured activations of multiple signaling pathways by using a high-throughput phosphospecific antibodies platform, 5-HT stimulated the extracellular signal–regulated kinase 1/2 (ERK1/2) in HUVEC. Moreover, we found that the physiological level of 5-HT induced phosphorylation of both ERK1/2 and eNOS in HUVEC. Human umbilical vein endothelial cell expressed both 5-HT_{2B} and 5-HT_{2C} receptors. SB204741, a specific 5-HT_{2B} receptor inhibitor, blocked 5-HT–induced ERK1/2 and eNOS phosphorylations, whereas RS102221, a specific 5-HT_{2C} receptor inhibitor, did not in HUVEC. SB204741 reduced microvessel density in tumors and inhibited the proliferation of HUVEC *in vitro*. These results suggest that regulation of 5-HT and 5-HT receptors, especially the 5-HT_{2B} receptor, may serve as a therapeutic strategy in cancer therapy.

Neoplasia (2009) 11, 408–417

Introduction

The results of clinical studies have thus far failed to show whether psychological factors affect cancer development [1]. We previously reported that emotions induced by hyperdopaminergic transmission, such as haloperidol-sensitive delirium, attenuate tumor growth [2,3]. The neurotransmitter serotonin (5-hydoxytryptamine [5-HT]) is causally involved in multiple central nervous facets of mood in regulating sleep, anxiety, alcoholism, drug abuse, food intake, and sexual behavior. The effect of 5-HT on tumor growth is still unclear [4–7]. Moreover, it has been reported that exogeneously applied high doses of 5-HT exert a direct mitogenic effect on tumor cells, whereas low doses of 5-HT reduce tumor growth by decreasing the blood supply to

Abbreviations: 5-HT, serotonin; 5-HTT, serotonin transporter; eNOS, endothelial nitric oxide synthase; LLC, Lewis lung carcinoma

Address all correspondence to: Satoru Ebihara, MD, PhD, Department of Geriatrics and Gerontology, Institute of Development, Aging and Cancer, Tohoku University, 4-1 Seiryo-machi, Aoba-ku, Sendai, 980-8575, Japan. E-mail: sebihara@idac.tohoku.ac.jp

[1]This study was supported by Grants-In-Aid for Scientific Research from the Ministry of Education, Science, and Culture of the Japanese government to M. A. (no. 19790553) and to S. E. (nos. 18014004 and 19590688).

[2]This article refers to supplementary materials, which are designated by Figures W1 and W2 and are available online at www.neoplasia.com.

Received 18 December 2008; Revised 21 January 2009; Accepted 21 January 2009

DOI 10.1593/neo.81630

the tumors [7], suggesting that the role of 5-HT on tumor growth is concentration-dependent on 5-HT. Among the subtypes of 5-HT receptors, which have been identified (5-HT_{1-7}) based on their structural, functional, and pharmacological characteristics [8], several subtypes have been found to exist in cancers [9–11]. The 5-HT_2 receptor subfamily consists of three members, i.e., 5-HT_{2A}, 5-HT_{2B}, and 5-HT_{2C} receptors. The 5-HT_{2B} receptor has been detected in many peripheral organs in several mammalian species including humans, primarily in the cardiovascular system, the gut, and the stomach fundus [12–18]. Especially, the blockade of 5-HT_{2B} is known to inhibit colon cancer and a prostate cancer cell line [11,19].

Nitric oxide (NO) is a major endothelium-derived relaxing factor [20]. Vasoconstriction is caused by activation of 5-HT_{1D} and 5-HT_{2A} receptors on vascular smooth muscle cells [21], whereas vasodilatation has been attributed to activation of 5-HT_{2B} receptors on endothelial cells, mediating the release of relaxing factors [22,23]. Endothelial nitric oxide synthase (eNOS), which produces NO in endothelial cells, plays a major role in inhibiting vasoconstriction to 5-HT [24,25]. Endothelial nitric oxide synthase is known to be stimulated by 5-HT [26]. Moreover, eNOS plays a role in the angiogenesis of tumor growth [27]. The levels of eNOS were found to increase in the carcinoma and to promote cancer progression by providing a selective growth advantage to tumor cells [28].

In peripheral tissues, 5-HT regulates vascular tone, gut mortality, primary homeostasis, and cell-mediated immune response [29,30]. Enterochromaffin cells produce and secrete far more 5-HT than either the central or the peripheral serotonergic neurons. The secreted 5-HT overflows to reach the peripheral blood by platelets [31–34]. Platelets, which do not synthesize 5-HT, are totally dependent on uptake to obtain 5-HT [30]. In 5-HT transporter (5-HTT) knockout mice, the level of 5-HT in the peripheral blood is virtually nil [34].

Although the concentration of 5-HT in the plasma has been shown to vary depending on psychological state, the level of hypertension, polymorphism in the 5-HTT-linked promoter region, and use of 5-HT reuptake inhibitors (selective serotonin reuptake inhibitors, SSRIs), the effect of a decreased level of 5-HTT on tumor growth has not been heretofore studied. Use of SSRI has been reported to reduce the risk of colorectal cancer in a large case-control study [35]. These studies suggest the existence of a strong relationship between 5-HT and cancer growth. Therefore, using *5-HTT*$^{-/-}$ mice, we investigated whether a decreased level of 5-HT affects tumor growth. In the present study, we found that specific inhibition of the 5-HT_{2B} receptor inhibited implanted lung cancer tumors in mice. On the basis of the analysis of a decreased level of 5-HT on tumor growth, we clarified the molecular mechanisms of the cancer inhibition by 5-HT_{2B} blockade.

Materials and Methods

Animals

Six- to 9-week-old male mutant mice lacking 5-HTT and littermate wild-type mice were obtained from heterozygous crosses with a 129Sv/C57BL6 mixed genetic background. Details of the generation of *5-HTT*$^{-/-}$ mice have been described previously [36]. We generated homozygous, heterozygous, and wild mice by crossing adult heterozygotes. DNA extract for tail biopsies were genotyped using polymerase chain reaction (PCR). Mice were group housed (two to four per cage) with food and water *ad libitum* in a room maintained at 22 ± 2°C and 65 ± 5% humidity under a 12-hour light-dark cycle. The animals were killed with an overdose of urethane (20 g/kg). All animal experiments were performed according to the Animals (Scientific Procedures) Act 1986 and approved by the local ethics panel at the Tohoku University School of Medicine.

Cell Culture

Lewis lung carcinoma (LLC), B16F0, and KLN205 cells were purchased from American Type Culture Collection (Manassas, VA). Lewis lung carcinoma and B16F0 cells were cultured in high-glucose Dulbecco's modified Eagle's medium containing 10% fetal calf serum, 100 U/ml penicillin, and 0.1 mg/ml streptomycin. KLN205 cells were cultured in minimum essential medium containing 10% fetal calf serum, 1% nonessential amino acids, and 100 μg/ml kanamycin. Human umbilical vein endothelial cells (HUVECs) were purchased from Kurabo (Osaka, Japan) and cultured in EC growth medium (Kurabo).

In Vivo *Tumor Models*

LLCs or B16F0 cells were injected (1×10^6 cells per animal) subcutaneously (s.c.) into the flank of male 6- to 9-week-old wild-type and *5-HTT*$^{-/-}$ mice on day 0. KLN205 cells were injected (5×10^5 cells per animal) s.c. into the flank of male 6- to 9-week-old BDF_1 mice on day 0. In solid-tumor growth experiments, paroxetine (20 mg/kg), fluvoxamine (20 mg/kg), SB204741 (*N*-(1-methyl-5-indolyl)-*N*-(3-methyl-5-isothiazolyl) urea), or RS102221 (8-[5-(5-amino 2,4-dimethoxyphenyl) 5-oxopentyl]-1,3,8-triazaspiro[4,5] decane-2,4-dione) (Tocris Cookson, Inc, Ellisville, MO) was injected intraperitoneally (i.p.) every 2 days from day 6. Tumor size was quantified daily as width^2 × length × 0.52. Mice inoculated with LLCs, those inoculated with B16F0 cells, and those inoculated with KLN205 cells were killed on days 23, 19, and 33, respectively. Control mice were treated with DMSO or saline.

Cell Proliferation Assays

The cell proliferation assay was performed as previously described [37]. Briefly, LLCs, KLN205, or HUVEC (5×10^3 cells) were plated onto 96-well plates and incubated with 0, 1, 10, and 100 μM SB204741 or RS102221. Each cell was cultured for 48 hours, and then the number of cells was determined by water-soluble tetrazolium assay using a cell counting kit (Dojindo, Kumamoto, Japan).

Detection of 5-HT Receptor mRNA by Reverse Transcription–Polymerase Chain Reaction Analysis

Total RNA was extracted from the cells using RNAzol B reagent (Tel-Test, Friendswood, TX) following the manufacturer's instructions. Reverse transcription–polymerase chain reaction analyses for 5-HT_{2A}, 5-HT_{2B}, and 5-HT_{2c} receptors were performed as previously described [21,38]. cDNA obtained by oligo-dT primed reverse transcription of total RNA isolated from HUVEC was subjected to PCR amplification with receptor-specific primers: 5-HT_{2A} receptor 5′-TCTTTAAGG-CGGGGAGTTGCT-3′ and 5′-TTTTGCTCATTGCTGATG-GACTG-3′; 5-HT_{2B} receptor 5′-TGCCATTCCAGTCCCTATT-3′ and 5′-GTGGATGT- TCTTCGCATAAGT-3′; 5-HT_{2C} receptor 5′-TGCATTCATTCCT- TGTGCAC-3′ and 5′-ATATCTAGG-TAGTGGCCAGA-3′; and the glyceraldehyde-3-phosphate dehydrogenase (*GAPDH*) 5′-GTCTTC- ACCACCATGGAGAA-3′ and 5′-ATCCACAGTCTTCTGGGT- GG-3′. Polymerase chain reaction products were separated by 1.5% agarose gel electrophoresis and visualized by ethidium bromide staining.

Protein Analysis

When the diameter of the tumor became 1 cm, tumor tissues were suspended in a lysis buffer (50 mM Tris-HCl, pH 7.4, 150 mM NaCl,

0.25% deoxycholic acid, 1% NP-40, 1 mM EDTA) containing protease inhibitors (20 mg/ml leupeptin, 1 mg/ml pepstatin A, and 1 mM PMSF) and then sonicated on ice. After centrifugation at 16,000*g* for 15 minutes, the supernatant was eluted in an SDS sample buffer (60 mM Tris-HCl, pH 6.7, 3% SDS, 2% 2-mercaptoethanol, and 5% glycerol) for 5 minutes. Next, 2×10^5 HUVECs were seeded in 10-cm dishes, cultured for 2 days, serum-starved (0.1% serum) for 24 hours, and then treated with various concentrations of 5-HT (0-50 μM). Cells treated with 5-HT or saline were suspended in a lysis buffer containing protease inhibitors and then sonicated on ice. Cell extracts were centrifuged, and the supernatant was boiled and subjected to 10% SDS-PAGE for transfer onto polyvinylidene difluoride membranes (Millipore, Billerica, MA). Each membrane was blotted with Abs to eNOS, phospho-eNOS (Ser 1177), extracellular signal–regulated kinase 1/2 (ERK1/2), and phospho-ERK1/2 (Cell Signaling Technology, Beverly, MA). Anti–5-HT_{2B} receptor, –5-HT_{2C} receptor, and –5-HTT were purchased from Santa Cruz Biotechnology, Santa Cruz, CA. The membranes were developed with an ECL Western Blotting Detection System Advance (Amersham Biosciences, Bucks, United Kingdom) according to the manufacturer's instructions. Phosphoprotein detection was performed by using the human phospho-MAPK assay Array kit (R&D Systems, Minneapolis, MN) according to the manufacturer's instructions. Image analysis was performed with ImageJ 1.37 software (National Institutes of Health, Bethesda, MD).

Immunohistochemistry

When the tumor diameter became 1 cm, under deep pentobarbital anesthesia (50 mg/kg body weight, i.p.), mice were perfused transcardially with 4% formaldehyde in a 0.1-M phosphate buffer. Tumor tissues were fixed in 10% formalin, embedded in paraffin, and sectioned. They were blocked with 10% normal goat serum and incubated with polyclonal antihuman factor VIII–related Ag Ab (Dako Japan, Kyoto, Japan). Subsequently, the sections were incubated with biotinylated goat antirabbit IgG (Vector Laboratories, Burlingame, CA), and then treated with the ABC kit (Vector Laboratories), for the detection of factor VIII–related Ag by 3-amino-9-ethylcarbazole (Vector Laboratories), and counterstained with hematoxylin.

Fluorescent Immunostaining

Sample preparation was the same as above. Sections (12 μm in thickness) were cut from the frozen tumor with a cryostat (CM1900; Leica, Heidelberg, Germany) and mounted onto glass slides (Dako, Carpinteria, CA). After incubation with 10% goat serum (Nichirei, Tokyo, Japan) for 1 hour at room temperature, the sections were incubated with mice monoclonal anti–factor VIII antibody (1:100) and rabbit polyclonal anti–phsopho-eNOS antibody (1:500; Cell Signaling Technology) for 36 hours at 4°C. Sections were subsequently incubated with fluorescein isothiocyanate–conjugated antimouse and Cy3-conjugated antirabbit IgG antibodies (1:100; Chemicon, Temecula, CA) for 1 hour at room temperature. Sections were then mounted on coverslips using antifade mounting medium (Vectashield; Vector Laboratories) and viewed using a confocal laser microscope (LSM 510; Carl Zeiss Meditec, Oberkochen, Germany).

Determination of Microvessel Density

Intratumoral microvessel density (MVD) was determined as previously described [37]. In brief, intratumoral vessels were stained immunohistochemically with antihuman factor VIII–related Ag Ab. The image that contained the highest number of microvessels was chosen for each section by initial scan at a magnification of ×100, and then the vessels were counted in the selected image at a magnification of ×200. At least four fields were counted for each section, and the highest count was then used. Two independent investigators evaluated the number of vessels.

Measurement of 5-HT

Serotonin was measured in the forebrain, tumors, and blood of wild type and *5-HTT*$^{-/-}$ mice. These samples were prepared as previously described [39]. The prepared samples from the forebrain, tumors, and blood were used for the assay of 5-HT by HPLC with electrochemical detection.

Cytokine Enzyme-Linked Immunosorbent Assays

The concentrations of vascular endothelial growth factor (VEGF) in the plasma, and cell culture supernatants were determined using a murine VEGF ELISA kit (R&D Systems) according to the manufacturer's recommendation. Lewis lung carcinomas or B16F0 cells were injected (1×10^6 cells per animal) subcutaneously (s.c.) into the flank of male 6- to 9-week-old wild-type and *5-HTT*$^{-/-}$ mice on day 0. Tumor size was quantified daily as width^2 × length × 0.52. Mice inoculated with LLCs were killed on day 23. The inferior vena cava of the mouse was then punctured, peripheral blood was collected, and plasma was isolated.

Data Analysis

Statistical analysis of the results was performed using analysis of variance (ANOVA) with Fisher's least significant difference test for multiple comparisons. A value of $P < .05$ was considered significant.

Results

Decreased Tumor Growth in 5-HTT *Knockout Mice*

The immunoblot analysis of implanted tumor homogenate by murine 5-HTT antibody showed the existence of 5-HTT in the *5-HTT*$^{+/+}$ mice but not in the *5-HTT*$^{-/-}$ mice (Figure 1*A*, *insert*). As shown in Figure 1, *A* and *B*, the tumor growth was markedly attenuated in *5-HTT*$^{-/-}$ mice. To test whether this growth might reflect a direct effect of 5-HT on LLCs or B16F0 cells, we examined the response of LLCs or B16F0 cell to 5-HT *in vitro*. We found that 5-HT did not increase LLCs or B16F0 cells proliferation *in vitro* (data not shown). To quantify tumor angiogenesis, we stained tumors with an antibody against the factor VIII–related antigen, a blood vessel marker (Figure W1) [40]. There was no difference in tumor MVD estimated by factor VIII–related antigen staining between *5-HTT*$^{-/-}$ and *5-HTT*$^{+/+}$ mice. Moreover, to examine the level of VEGF in the culture supernatant fluid, we performed enzyme-linked immunosorbent assay. There were no differences among LLCs and B16F0 cells with 5-HT or saline treatment (data not shown).

Decreased Level of 5-HT in Tumors of 5-HTT$^{-/-}$ *Mice*

We reported that *5-HTT*$^{-/-}$ mice displayed reduced levels of 5-HT in the frontal cortex [36]. Next, we focused on 5-HT analyses of the tumor and peripheral blood. Mice lacking 5-HTT were generated, and either LLCs or B16F0 cells were injected (1×10^6 cells per animal) s.c. into the flank of both *5-HTT*$^{-/-}$ and *5-HTT*$^{+/+}$ 6-week-old mice

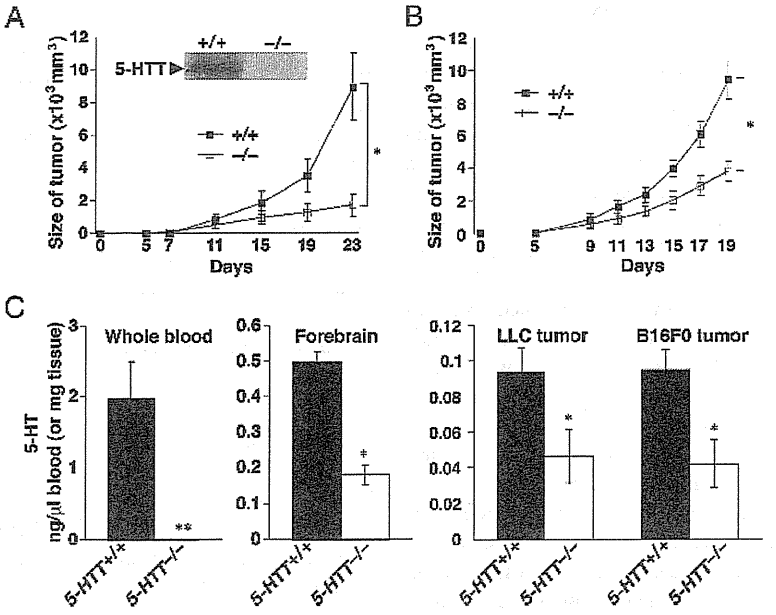

Figure 1. Effects of 5-HT on tumor growth in mice. (A) A total of 1 × 10^6 LLC cells were implanted into *5-HTT*$^{-/-}$ and *5-HTT*$^{+/+}$ mice. Tumor volumes were calculated from tumor measurements scored on the indicated day. Results are presented as the mean tumor volume ± SD (n = 6, 7 per group). Insert shows Western blot analysis of 5-HTT protein in tumors of *5-HTT*$^{-/-}$ and *5-HTT*$^{+/+}$ mice. (B) A total of 1 × 10^6 B16F0 cells were implanted into *5-HTT*$^{-/-}$ and *5-HTT*$^{+/+}$ mice. Tumor volumes were calculated from tumor measurements scored on the indicated day. Results are presented as the mean tumor volume ± SD (n = 6 per group). (C) Serotonin in whole blood, forebrain, and tumors of *5-HTT*$^{-/-}$ and *5-HTT*$^{+/+}$ mice on day 23 (LLC) after implantation. Serotonin in tumors of *5-HTT*$^{-/-}$ and *5-HTT*$^{+/+}$ mice on day 19 (B16F0) after implantation. Values represent the mean ± SD (n = 6, 7 per group). Statistically significant (*P < .05, **P < .01) compared with *5-HTT*$^{+/+}$ mice.

on day 0. The tumor size was quantified daily, and mice were killed on day 23. As shown in Figure 1*C*, in *5-HTT*$^{-/-}$ mice bearing LLC tumors, electrochemical detection of 5-HT showed a level of 5-HT in the blood below the level of detection. Serotonin levels in the forebrain of *5-HTT*$^{-/-}$ mice bearing LLC tumors were significantly lower than those of their *5-HTT*$^{+/+}$ littermates with LLC tumors. Serotonin levels of LLC or B16F0 tumors were also significantly lower in *5-HTT*$^{-/-}$ mice than in *5-HTT*$^{+/+}$ mice.

5-HTT Inhibitors Did Not Decrease Tumor Growth

It has been reported that 5-HTT inhibitors inhibit cancer initiation by inhibition of 5-HT reuptake [41]. We thus investigated whether the 5-HTT inhibitors influence tumor growth. Lewis lung carcinoma cells were inoculated into the flank of C57BL/6J mice s.c. on day 0. From day 6 after tumor identification, we i.p. injected paroxetine, a 5-HTT inhibitor; fluvoxamine, a 5-HTT inhibitor; or saline every 2 days. Compared with saline treatment, paroxetine or fluvoxamine treatment did not inhibit tumor growth (Figure 2*A*). Moreover, we investigated the influence between 5-HTT inhibitors and another cancer cell line, KLN205. In the KLN205 tumor growth model, there were no differences between saline treatment and 5-HTT inhibitors (Figure 2*B*). Serotonin levels in the whole blood of mice treated with paroxetine or fluvoxamine were significantly lower than those of mice treated with saline (Figure 2*C*), but the 5-HT levels in tumors did not differ among saline-, paroxetine-, and fluvoxamine-treated mice (Figure 2*D*). These results suggest that levels of 5-HT in the tumor but not in the whole blood might influence tumor growth.

Decreased eNOS Expression in 5-HTT$^{-/-}$ *Mice*

Because eNOS plays a major role in inhibiting contraction of arteries to 5-HT, we next investigated the expression of eNOS in LLC tumors from *5-HTT*$^{-/-}$ mice, which had 5-HT levels in the whole blood. We found that eNOS protein expression in tumors was lower in *5-HTT*$^{-/-}$ mice than in *5-HTT*$^{+/+}$ mice (Figure 3*A*). As shown in Figure 3*B*, stimulation with 5-HT (1-50 μM) for 24 hours induced eNOS expression in HUVEC in a concentration-dependent manner. Next, we investigated whether 5-HT induced signaling pathways in HUVEC. According to previous reports, 5-HT induced phosphorylation of MAPK and Akt in various cell types [42]. However, HUVEC has not been studied yet. We measured the phosphorylation of multiple signaling pathways by using a high-throughput phosphospecific antibodies platform. Human umbilical vein endothelial cells were treated with or without 1-μM 5-HT, and cell signaling was assessed. As shown in Figure 3*C*, 5-HT stimulation modulated the ERK1/2 in HUVEC. These results suggest that 5-HT stimulation may induce eNOS expression through the ERK1/2 phosphorylation in HUVEC.

Stimulation of 5-HT$_{2B}$ Receptor Induced the Phosphorylation of eNOS through ERK1/2 in HUVEC

Phosphorylation of eNOS produced more bioavailability of the signaling molecule nitric oxide (NO) than eNOS. Endothelial nitric oxide synthase is phosphorylated in response to various forms of cellular stimulation in endothelial cells [43]. In the present study, we investigated whether eNOS phosphorylation was induced by 5-HT in HUVEC in detail. We stimulated HUVEC with various concentrations of 5-HT for 10 minutes. phosphorylations of ERK1/2 and

eNOS were concentration-dependent of 5-HT (Figure 4*A*). As shown in Figure 4*B*, 1-μM 5-HT caused transient phosphorylation of both ERK1/2 and eNOS. Next, we examined the effect of U0126 or PD 98059, which are ERK1/2 inhibitors, on 5-HT–induced ERK1/2 phosphorylation. Human umbilical vein endothelial cells treated with U0126 or PD 98059 blocked not only ERK1/2 phosphorylation but also eNOS phosphorylation (Figure 4*C*). Moreover, we investigated what types of 5-HT receptors induced ERK1/2 phosphorylation in HUVEC. Reverse transcription–polymerase chain reaction and Western blot analysis revealed that 5-HT_{2B} and 5-HT_{2C} receptors were expressed in HUVEC (Figure 4, *D* and *E*). SB204741, which is a specific 5-HT_{2B} receptor inhibitor, blocked 5-HT–induced ERK1/2 and eNOS phosphorylation, whereas RS102221, which is a specific 5-HT_{2C} receptor inhibitor, did not (Figure 4*F*). These results suggest that the 5-HT_{2B} receptor plays a pivotal role in HUVEC and that inhibition of the 5-HT_{2B} receptor may reduce tumor growth.

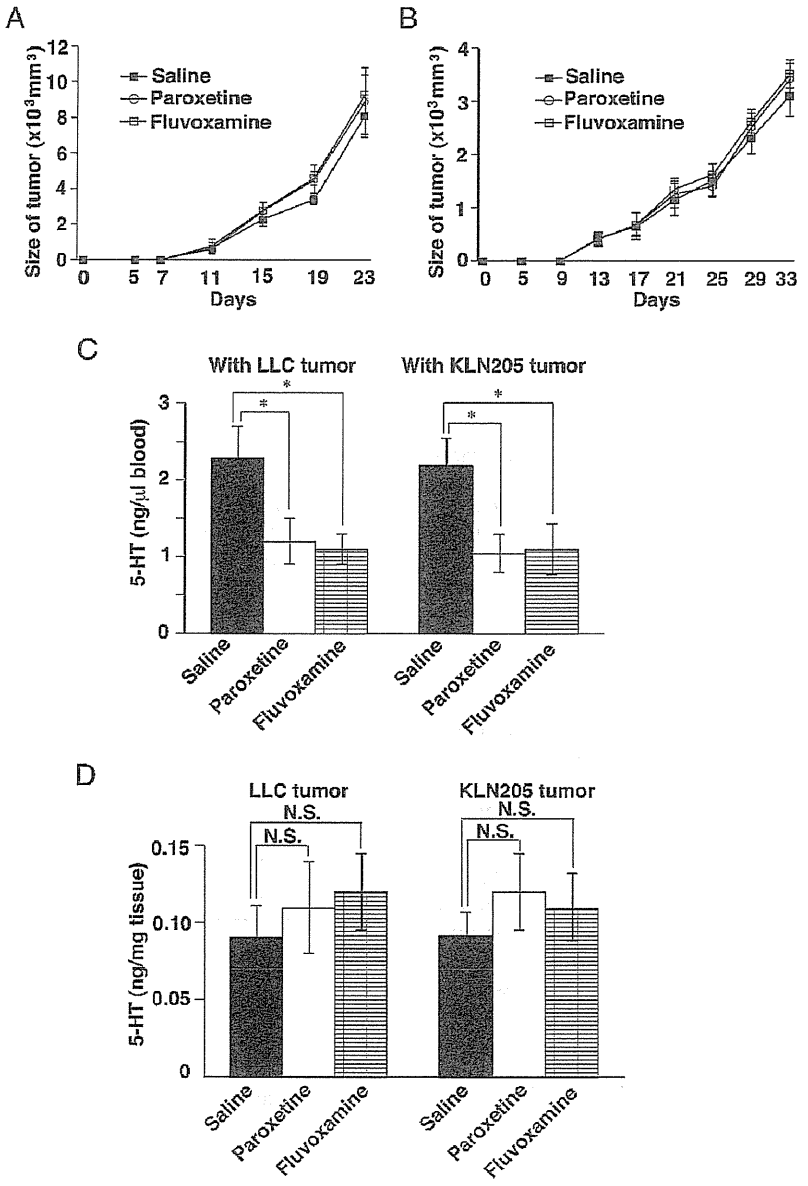

Figure 2. Paroxetine and fluvoxamine did not decrease tumor growth. (A) Mice were injected s.c. with LLC on day 0 and were treated with saline (closed squares), paroxetine (circles), or fluvoxamine (open squares) from day 6, every 2fs days. (B) Mice were injected s.c. with KLN205 on day 0 and were treated with saline (closed squares), paroxetine (circles), or fluvoxamine (open squares) from day 6, every 2 days. Tumor volumes were calculated from tumor measurement scored on the indicated day. Results are presented as the mean tumor volume ± SD. (C, D) On day 23 (LLC) or 33 (KLN205) after implantation 5-HT in whole blood and tumors of mice with paroxetine, fluvoxamine, or saline. *Statistically significant ($P < .05$) compared with saline-treated mice. The values represent the mean ± SD ($n = 8$ per group).

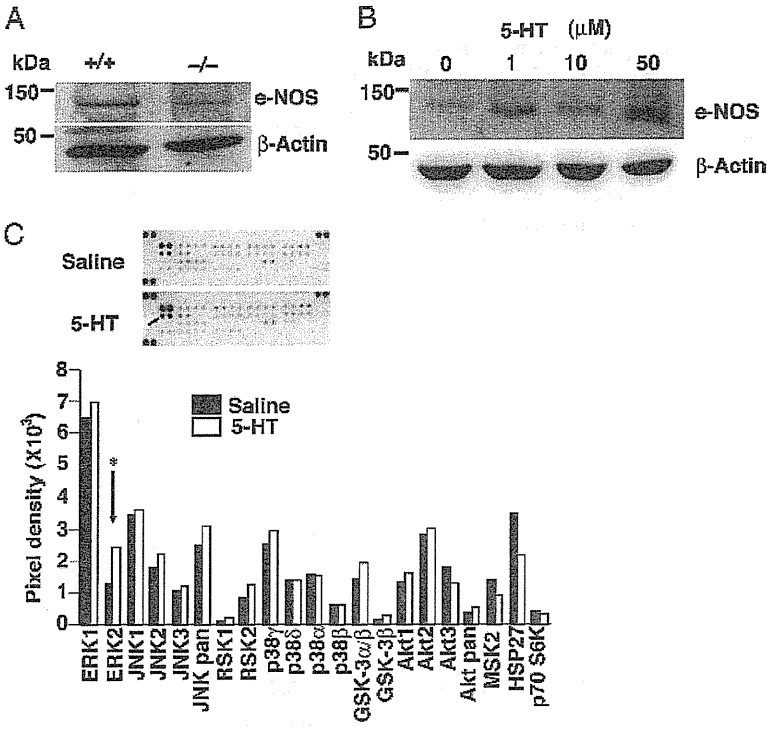

Figure 3. Association between 5-HT and eNOS. (A) LLC tumors from *5-HTT*$^{-/-}$ mice decreased eNOS. (B) Effects of 5-HT on 5-HT–induced eNOS in cultured HUVEC. Serotonin or saline was added to cultured HUVEC for 24 hours. Cells were collected for extraction and immunoblot analysis with antibodies to eNOS and β-actin. (C) Effects of serotonin on 5-HT–induced signaling pathways in cultured HUVEC. Saline or 5-HT, 1 μM, was added to cultured HUVEC for 10 minutes. Phosphorylation of intracellular signaling molecules was assessed by using the human Phospho-MAPK Array kit. The columns present the results of the densitometric analysis of the dot images corresponding to the phosphorylation status of individual protein. *Statistical significance was determined by 2-tailed-Student's *t* test.

SB204741 Reduced Tumor Growth

We investigated whether inhibition of the 5-HT_{2B} receptor influenced tumor growth *in vivo* because the 5-HT_{2B} receptor antagonist reduced 5-HT–induced ERK1/2 and eNOS phosphorylation. KLN205 cells were inoculated into the flank of BDF_1 mice s.c. on day 0. From day 6 after tumor identification, we injected SB204741 (20 mg/kg), RS102221 (20 mg/kg), or DMSO, as a control, i.p. every 2 days. Compared with DMSO treatment, SB204741 treatment inhibited tumor growth (Figure 5*A*). Similar results were obtained from the inoculation of LLCs (Figure 5*B*). We next examined the direct effect of SB204741 or RS102221 on the proliferation of HUVEC, LLCs, and KLN205 cells with various concentrations of these inhibitors. SB204741 reduced the proliferation of HUVEC and KLN205 cells *in vitro* (Figure W2). These results suggest that SB204741 reduced tumor growth because SB204741 inhibited the proliferation of the endothelial cells and KLN205 cells.

SB204741 Treatment Decreased Blood Vessel Density in Tumor Tissues

Hematoxylin and eosin staining of the tumor tissues revealed a decrease in vessels in KLN205 and LLC tumor tissues taken from SB204741-treated mice (Figure 5, *C* and *D*). To confirm the vessels, we stained paraffin sections immunohistochemically using an antibody against factor VIII–related Ag. Compared with DMSO-treated mice, we found fewer tumor vessels in SB204741-treated mice. The localization of phospho-eNOS in the LLC tumor tissues was determined by fluorescent immunostaining (Figure 6*B*). Immunostainning of phospho-eNOS was observed in the endothelial cells and completely overlapped that of factor VIII–related Ag. The differences in MVD between control and SB204741 mice were statistically significant (Figure 6*A*).

Discussion

This is the first study to extensively examine the effect of depletion of 5-HT on tumor growth *in vivo*. Conflicting results have been reported on the effect of exogeneously applied 5-HT on tumor growth [6]. In this study, we therefore investigated the effect of a low level of 5-HT, i.e., which is lower than the physiological level of 5-HT, on tumor growth. Using 5-HTT–deficient mice, we found that 5-HT levels in the tumor played a crucial role in tumor growth, suggesting that physiological levels of 5-HT in the tumor are needed for tumor growth. In addition, we found that SB204741, which is a 5-HT_{2B} receptor inhibitor, suppressed the phosphorylation of ERK1/2 and eNOS in HUVEC. Moreover, we found that SB204741 reduced tumor growth by suppressing angiogenesis.

Although the inoculated cancer cells were not knocked out of 5-HTT, there was no 5-HTT protein in tumors implanted in 5-HTT mice, suggesting that the 5-HTT protein is completely absent in our 5-HT depletion models. Other methods to deplete 5-HT, such as deleting enzymes involved in 5-HT synthesis (tryptophan hydroxylases),

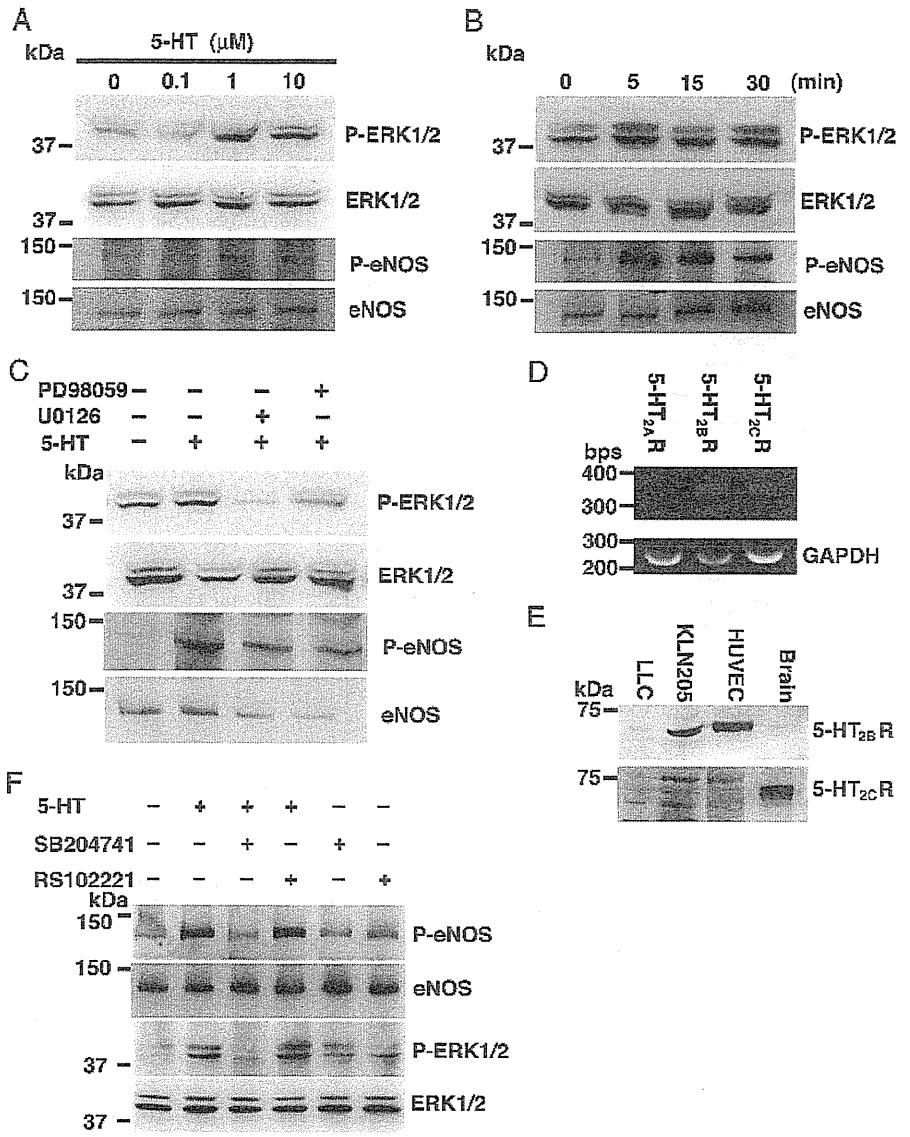

Figure 4. Stimulation of 5-HT_{2B} receptor induced the phosphorylation of eNOS through ERK1/2 in HUVEC. (A) Effect of doses of 5-HT incubated for 10 minutes on phosphorylation of ERK1/2 and eNOS in HUVEC. (B) Serotonin induced activation of ERK1/2 and eNOS. Human umbilical vein endothelial cells were treated with 1-μM 5-HT for the indicated time. (C) Inhibition of ERK1/2 activity by U0126 and PD98059. Human umbilical vein endothelial cells were preincubated with 10-μM U0126 or 10-μM PD98059 for 30 minutes, then treated with 1-μM 5-HT for 5 minutes. (D) Reverse transcription–polymerase chain reaction analysis of selected 5-HT receptors in HUVEC. The bands representing the 5-HT_{2A} receptor (301 bp), the 5-HT_{2B} receptor (363 bp), the 5-HT_{2C} receptor (354 bp), and GAPDH (268 bp) are indicated. (E) Western blot analysis to demonstrate the expression of 5-HT_{2B} and 5-HT_{2C} receptors in LLC, KLN205, and HUVEC. The proteins were detected with polyclonal 5-HT_{2B} receptor and polyclonal 5-HT_{2C} receptor antibodies. Mice forebrain expressed 5-HT_{2B} and 5-HT_{2C} receptors as a positive control. (F) Inhibition of ERK1/2 activity by SB204741. Human umbilical vein endothelial cells were preincubated with 10-μM SB204741 or 10-μM RS102221 for 30 minutes, then treated with 1-μM 5-HT for 5 minutes. Phosphorylation of ERK1/2 and eNOS was determined by Western blot analysis using phosphospecific antibodies.

may not work as long as LLC and B16F0 have the enzyme. If we knock out the enzyme in LLC and B16F0, we cannot exclude the possibility that the absence of the enzyme affects the proliferation and synthesis of LLCs and B16F0 cells.

Selective serotonin reuptake inhibitors are the most commonly prescribed drugs for treating depression. Therefore, the effects of SSRIs on cancer have been studied. Although it has been reported that SSRIs have cytotoxic activity against colorectal cancer [7,41,44], our results showed that paroxetine and fluvoxamine did not reduce tumor growth *in vivo*. Selective serotonin reuptake inhibitors are known to decrease whole-blood 5-HT concentrations in patients [45]. In this study, although paroxetine and fluvoxamine decreased the whole blood 5-HT concentration, it did not influence the 5-HT level in the tumor. These results suggest that the 5-HT levels in the tumor could be important, whereas SSRIs might have a different influence in each cancer type [44].